



Stability analyses of dams using multidisciplinary geoscience approach for water reservoir safety: case of Mpu Damsite, Southeastern Nigeria

S. N. Ukpai¹

Received: 19 April 2020 / Accepted: 18 September 2020 / Published online: 19 November 2020
© Springer-Verlag GmbH Germany, part of Springer Nature 2020

Abstract

Geological, hydrological, and geotechnical conditions affected water reservoir safety at the studied damsite. Geophysical and hydrogeological surveys were integrated with hardness test, geological strength index (GSI), rock mass rating (RMR), and shear and compressive strength analyses of bedrocks. Fresh bedrocks were identified at minimum depth of about 10 m with resistivities ranging from 1670 to 4539 Ohm m for the respective argillaceous Ezeaku Group and indurate Asu River shales; both depicted 54 and 47.5 of RMR consecutively. Further results showed very blocky and slightly weathered bedrock, uniaxial compressive strength (UCS) ≥ 20 MPa, mean point load index of 9.3 MPa, and allowable bearing capacity (q_{al}) > 21 MPa. The bedrock qualities were certified fair for bearing dam loads, hence, signified competence as stable bearing surfaces, but devastated due to exposure to oxidation processes introduced by seepages through clay/siltstone that overlies bedrocks as composite layer. Then, uplift pressure (P_u) was initiated, resulting in failure modes. Predictably, occurrence of critical exit gradient and eventual general failure is envisaged due to vigorous leakage into the foundation zone from settling tail water portion. Panaceas should include $P_u \ll D_w$ (dam weight), grouting the leakage zones with concretes of UCS ≈ 20 MPa, and piling into deep foundations.

Keywords Damsite · Seepages · Uplift pressure · Dam foundation · Composite bedrock · Reservoir safety

Introduction

Background to the study

Climatic change due to global warming drives hydrologic system to extreme events like flooding and drought (Sivakumar 2011). Adverse effects of these components have been impeding the economy of developing nations, in terms of sustainable freshwater supply for food production, in energy sector and domestic works. For instance, over the past 105 years that temperature has increased by 1.1 °C, annual rainfalls have decreased by 81 mm (Akpaodiogaga and Ovuyovwiroye 2010) resulting in longer period of drought than annual duration of flood characteristic rain falls in Africa. Consequently, perennial streams and rivers are

increasingly modifying to ephemeral conditions, thus lessened crop production, slowed both services in industries and economic activities, particularly around southeastern Nigeria. The region is the economic stronghold of the nation through palm oil, kernel oil, and rice production. Because the underlying geology is dominated by mineralized rocks (Obaje 2009) and low permeable sediments that spanned from Lower Benue Trough to Anambra Basin (Appendix 1), occurrences of alternative water supply from groundwater resource have been hampered. This raised serious concern on need for safe and sustainable freshwater supply. But then, dam has been seen as an effective way of meeting water and energy needs (Altinbilek 2002). Therefore, this study considered the importance of dam in the sustainable freshwater development through water reservoir scheme (Fig. 1a, b), hence, focused on its stability analysis for the reservoir safety with respect to economies, lives, and properties of adjoining environments using Mpu Damsite as a typical case.

The dam was constructed across a tributary of River Asu, which produced water reservoir (Fig. 1) that supplies almost 90% of freshwater distributed in the region. However,

✉ S. N. Ukpai
ukpaisteve@yahoo.com

¹ Department of Geology, Ebonyi State University, Abakaliki, Nigeria

Fig. 1 The dammed water reservoirs. **a** Axis showing the downstream end of traverse line 1 between reservoir I (R-I) and reservoir II (R-II) and the upstream edge of traverse line 2. **b** Embankment demarcating reservoir I and II. **c** Downstream edge of traverse line 2 along the failing section of the dam by the tail water (R-III)



construction of dams has always been accompanied by negative impacts that pertain loss of ecosystem (Beck et al. 2012). In such manner, Ezeigbo (2003) reported that large volume of water released from the Nigerian Kainji Dam caused real environmental havocs. This is because dam failures inflict flooding that does not only destroy biodiversity and displace local populations within the vicinity (Boyč and de Vivo 2016) but devastate nearby farmlands. Environmental hazards of this kind are therefore imminent around the flood plain of the studied damsite due to envisaged failure scenario from observed embankment settling or defect (see Fig. 1c). The failure mode heaved the dam by streamlining confined flow or leakage “termed in this study as secondary seepage” into the foundation zone. It means that the failure mode was either initiated by primary seepage from unconfined flow through an underlying geologic structure, or by other means of geotechnical instability (Fig. 2).

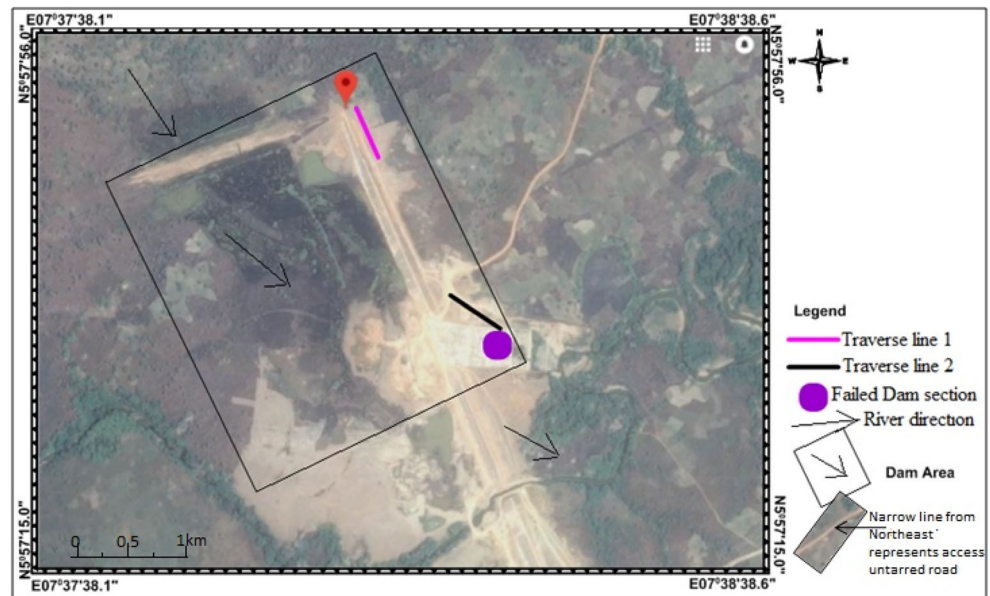
For these reasons, geotechnical condition of the studied site was critically investigated. Acquired dataset related the problematic situation of the failing dam with engineering-geological properties of the underlying shaley bedrock. The shales are confined by a composite clay layer and sandwich the clay around geologic formation boundary underneath the dam where the bedrock weathered. This is the major source of risks that degenerated to devastation of foundation bearing via seepage-induced uplift pressure and local shear failure. The fact that piezometric pressure at the foundation zone is related to water seepage (Shah Shahrbanouzadeh et al. 2015) consequent upon which high moisture content may be

confined, the fundamental aim of this study was to identify the primary seepage pathways and the geotechnical significance. Findings in the present study would draw awareness of specific sources of such conditions that lead to dam failures in order to foreclose any related downside.

According to Fooks and Lee (2019), availability of moisture and extent of moist conditions in structures around hot climatic regions induce salts (i.e., dissolved solutes) which weaken concretes by means of reinforcement corrosion. Based on this concern, especially as the studied region has been characterized by typical tropical climate, the scope of this research comprised investigation for confined moisture contents within the foundation and the consequent hydrogeochemical status, as well as the extent of imparted weakness on the dam load bearing surfaces. Singh and Goel (2011) had highlighted that any foundation resting on weak rock surfaces poses serious failure problems. The worst scenario arising from dam-related geotechnical instability was reported by Costa (1985) as fatalities of human lives. In this case, risk-based guidelines ought to have been provided during design stage before construction (Pan and Fu 2020) to avoid the failure consequences, perhaps due to inadequate geological investigation (Sissakian et al. 2020).

During preliminary inspection of the damsite, some observed instability sources suspected as smash points that had even caused failures in previous works include the following: headcut erosion (Wahl 1998), foundation crack or defect (ASDSO 2019) in form of sagging at the toe, and physical characteristics of the damsite (NYSDEC 2009) in terms of

Fig. 2 Google Earth imagery of the damsite at a syncline where Asu River Group overlapped with Ezeaku Group (with a NE-SW fracture trace crossing an untarred road at the Northeastern part of the image)



geomorphology. Mitigating these factors would improve public safety and resilience around the damsite (ASCE 2017). For this reason, detailed information relating to the risk sources were explored using integrated geotechnical, geological, hydrological/hydrogeological, remote sensing, electrical resistivity, and other geophysical surveys. This is because Panthulu et al. (2001) delineated seepage paths in dam foundation using electrical resistivity method. Similarly, damsite can be characterized using geophysical and hydrological analyses (Chu et al. 2013), such as induced polarization (IP) for engineering and environmental studies for detection of vertical cavities (Loke 2001) and underground voids (Sheets 2002). Previously, IP has been successfully used for detection of clayey and shaley sediments (Klein and Sill 1982), even as Fetter (2007) explained successful use of fracture trace analysis to investigate stability of sediments bearing dam foundations. Even with these previous studies, Zainab et al. (2007) reiterated that much has not been studied to address some issues relating to tropically weathered anisotropic and non-homogenous sedimentary rocks.

The present study therefore combined these surveys and focused on rock mass rating (RMR), fracture tracing analysis, moisture/pore water pressure and hydrogeochemical analyses of the foundation zone, and shear and compressive strengths analysis of the rock heads, as well as self-weight effect of the dam on the bearing bedrocks. Results of the study emphasized the need to identify unweathered composite bedrock that can form stable bearing surface at depth. Moreso, as low effective stress characterizes strain modulus of uncemented clay (Vardanega and Bolton 2013) and because cement-treated clay tends to remain intact under unconfined load (Yao et al. 2020) especially as evaluation of the cement-treated clayey subgrades could be conducted with unconfined (uniaxial)

compression test (Yao et al. 2019), unconfined compressive strength (UCS) determined in the intact shale should be equivalently used in gauging cement admixed grouts to consolidate the clayey and leakage-forming weathered portion of the dam foundation. Pan et al. (2017) had proposed jet-grouting in typical remedial approach, particularly in construction of cut-off walls. Meanwhile, penetrating diaphragm cut-off wall in the seepage direction could fit the best remedy (Pan and Fu 2020). The present study suggested both scenarios, even though expensive but cost-effective. The entire findings could be sufficiently used comparatively to check stability of embankments in general cases of related water reservoir schemes, even in larger hydro dams.

Regional tectonic, stratigraphic, and geomorphologic setting

Breaking-up of Gondawana supercontinent in late Jurassic vis-a-vis separation of South American plate from that of Africa (Nwajide 2005), created three rift (R) arms that formed triple “R” junction (Wright 1989). While two of the rift arms drifted to equatorial ocean (Burke and Whiteman 1973; Burke and Dewey 1974) and South Atlantic Ocean (Benkhelil 1989), the third arm could not drift further than to become a failed rift that opened into West Africa, particularly towards Nigeria. The failed rift with width upto 250 km stretches to a length of about 1000 km across Nigeria (Ofoegbu et al. 1990) forming an elongated NE-SW trending depression referred as Benue Trough (Burke et al. 1970). The trough is geographically subdivided into lower, middle, and upper portions (Peters and Ekweozor 1982; Idowu and Ekweozor 1993), although with no concrete line of subdivision except with defined geographical locations. The lower portion referred by Nwajide (2013) as southern

Benue Trough encompasses Abakaliki anticlinorium, Afikpo syncline, and Mamfe embayment, as well as Gboko and Ogoja areas. Sedimentary deposits in these depocenters constitute cretaceous sediments that comprised Asu River Group of Albian, Odukpani Formation of Cenomanian, Ezeaku Group of Turonian, and Awgu Formations of Coniacian (Akanke et al. 1992; Idowu and Ekweozor 1993). The Asu River Group is mainly shales with intercalations of siltstone, limestone, and sandstones around Abakaliki Region. Due to absence of the Cenomanian sediments in areas around the anticlinorium, Umeji (1984) reported that Asu River Group was unconformably overlain by shale bedrocks, siltstones, and sandstone units that belong to Ezeaku Group. The sediments of Ezeaku Group and younger cretaceous sediments overlap with the oldest Asu River shale deposited towards Ishiagu area (Okogbue and Ukpai 2013) along the axis of the Anticlinorium and extended downdip in SW-NE orientation (Ukpai et al. 2016) across Mpu district from Abakaliki Region.

Materials and methods

Preliminary outlook of the damsite was provided from the Google Earth image (version 7.3) for the acquisition of space-based images of the environment as recommended by United States Geological Survey (USGS 2016). Linear features earlier delineated by Ukpai (2018) in refined data from Nigerian Geological Survey Agency (NGSA) for map sheet 302 which covered the adjoining region were juxtaposed to the imaged Google Earth scene of the damsite for fracture trace analysis. Detailed ground proving was undertaken via integrated field mapping, which commenced with lithofacies analysis at outcrops, roadcuts, river banks, and in cored samples. Rocks hardness test was roughly examined in situ by stroking on the outcrops via geological hammer blow in line with specifications of ISRM (2007). The test was followed by determining geological strength index (GSI) being proposed by Roclab (2006), as well as Marinos and Hoek (2000) based on visual inspection of surface geological condition to estimate strengths of the outcropped rock mass around the damsite.

Configuration of apparent resistivity curves from 1D electrical sounding was used for preliminary delineation of water table around the damsite. ABEM Terrameter was used for the survey via Schlumberger array in azimuthal NW-SE direction for about six (6) stations. Separately, combined vertical electrical sounding and induced polarization (VES-IP) survey in a single 2-D platform was carried out for delineation of underlying bedrock via Wenner-Schlumberger array using Geomatic instruments (GD-20 model). The acquired 2D data were subjected to inversion technique using RES2DINV program for subsurface geologic tomogram. The tomographic imaging followed guidelines stated in relevant literature, particularly Zhou et al. (2014) and Lelièvre and Farquharson

(2013). Two dimensional (2D) survey of this kind identifies subsurface mound of electrical conductivity of geologic materials beneath dam terrace (Chu et al. 2013). The 2D data was collected perpendicular to the dam embankments and parallel to the river channel in two traverse lines, namely traverse 1, from upstream section of the dam across heel heads **i** and **ii** (H-**i** and H-**ii** reservoirs), while traverse 2 connected the end of traverse 1 to downslope section around tailwater head (H-**iii**). Trends of the traverses were designed to crisscross the major geological formations (see Fig. 4) in order to delineate rock heads underneath the dam. Multi-electrodes (16 current (C) and 16 potential (P)) were set up via Wenner-Schlumberger array. Spacings between P1 and P2 were kept at “a” while wider spacing “na” between C1 and P1, as well as between C2 and P2 was increased with respect to separation factor “n,” for “n” = 1, 2, and 3.

Composite shale strengths were specifically determined based on the most preferable and reliable in situ test in agreement with Zainab et al. (2007) by coring into the bedrocks for geotechnical quality test. Thus, the test commenced with extraction of block cored samples from rock heads by drilling method (Appendix 3). The analysis followed thus:

Rock mass rating (RMR) was estimated via summation (Σ) of parameters in Eq. (1) in order to predict rock mass behavior, hence (Wang et al. 2016):

$$\text{RMR} = \text{R1} + \text{R2} + \text{R3} + \text{R4} + \text{R5} + \text{R6} \quad (1)$$

Each parameter is defined as follows: uniaxial compressive strength or strength of rock substance (R1); rock quality designation, RQD (R2) from solid cylindrical core samples; groundwater condition (R3); and fracture (orientation [R4], spacing [R5], condition [R6]). The RQD was based on fresh rock samples cored from drilled holes as typically shown in Appendix 3.

From macroscopic view of outcrops, slight fracturing of the underlying bedrocks was suspected, hence, the estimation of ultimate bearing pressure (q_{ult}) using Goodman (1989) Eq. (2):

$$q_{ult} = q_c (N_\phi + 1) \quad (2)$$

where:

$$N_\phi = \tan^2 \alpha \quad (3)$$

and

$$\alpha = (45 + \phi'/2) \quad (4)$$

The allowable bearing pressure (q_{al}) was estimated as:

$$q_{al} = q_c (N_\phi + 1) / \text{FS} \quad (5)$$

Taking FS as factor of safety,

N_ϕ bearing pressure factor,

ϕ friction angle of intact rock (angle of shear strength).
 q_c uniaxial compressive strength (UCS), particularly used to estimate bedrock stability against load (Gholami and Fakhari 2017) such as the dam, and was performed on cylindrical cored samples as suggested by Brown (1981). In line with Sivakugan et al. (2014), this parameter could directly be determined from uniaxial compression test. Accordingly, compression test apparatus (UK Comtest 3000 kN model) was used for the set-up. The test commenced by measuring the diameter D and length L of the cored cylindrical samples with a vernier caliper, while those of $D/L \geq 2$ were selected as specimen for the test. This precaution was taken in accordance with Briaud (2013) to ensure that oblique shear plane that usually develops on the specimen during failure propagated across the specimen dimensions without intersecting the two platens. None of the specimen was confined during the tests in order to keep horizontal (minimum) principal stress at zero, while a uniform vertical pressure was applied as principal stress by pushing up the bottom platen in order to compress upon longitudinal circular cross-section of the specimen against a load (in kN) hinged on the loading device by the top platen. The top platen was held in a fixed position while constant rate of displacement was maintained by gradual increase of the vertical stress until failure occurred. The vertical stress at failure was read off from pressure transducer tool of the equipment and was recorded as the UCS.

For the fact that the set-up is randomly same with axial test, especially as it is equipped with point load test (PLT) accessories, other shear strength parameters relevant to this study were determined using the PLT principle. It was even used as indirect means of predicting the UCS. According to ISRM (1981), PLT is an outstanding reliable means of determining UCS. This test was performed on separate cored shale samples but from same borehole (BH) sources with specimen used for direct test earlier used to measure UCS. However, the lengths (L) of the PLT specimens were saw cut to half size of the L earlier used for the compression test, such that L/D is within 0.3 and 1.0 specified by ASTM and ISRM for axial test. Each sample specimen was placed in testing chamber between the two conical steel platens and gradually compressed under pressure with loading until major cracks or splitting (otherwise failure) occurred after an average period of 120 s. At splitting point, amount of compressing load was read off from the pressure gauge and recorded as point load (P) in kN. The failure cracks (splits) were manually traced on each residually stressed specimen and the inclination angles measured with protractor (half circle) while the mean was recorded as angle of failure, α . Contact of the upper and lower platens on the specimen after failure was traced to a vertically positioned scale tool of the PLT equipment and read off as diameter at maximum displacement (D), even as the

equivalent diameter (D_e) was measured with caliper before the test. The point load strength index (I_s) was evaluated from Eqs. (6–7) and correlated to UCS by a coefficient factor (Eq. (8)). Rusnak and Mark (1999) had proposed 21.9 as conversion factor for typical shales, even as various literatures suggested a range from 20 to 25 (Osouli et al. 2014). In order to determine suitable minimum UCS in cement-treating clay laden weathered portion of the shale at the shear axis of the dam foundation, the present study chose 22 being an approximated mean of the conversion factors for shales to predict the UCS of the underlying bedrock, thus:

$$I_s = (P \times 1000)/D_e^2 \text{ (MPa)} \quad (6)$$

However, Eq. (6) was corrected to (7) for the purpose of core size fitting with respect to standard 50 mm diameter for D_e , hence:

$$I_{s50} = (P \times 1000)/(D_e^{1.5} \times \sqrt{50}) \text{ (MPa)} \quad (7)$$

therefore;

$$\text{UCS} = 22 * I_{s50} \text{ (MPa)} \quad (8)$$

Mutually, the predicted and measured UCS was graphically compared with reference to Yao et al. (2020) to establish confidence on equality of both test outcome.

The water table was ground confirmed with the aid of dip meter (Heron model) by measuring static water levels in open drilled holes (Ukpai et al. 2016) earlier used for coring (see Appendix 3a) after 48 h of core sampling. In order to ascertain geochemical status of the foundation zone, physico-chemical parameters, mainly EC, TDS, and PH in groundwater sampled from the cored holes, were measured in situ using a portable WTW LF 90 conductivity/TDS/PH meter. For the fact that the studied area is ferruginized and iron-banded terrain, a sample was collected with 1-l sample bottle from each drilled hole and at the ponded surface water around heel head II of the reservoir for analysis of dissolved iron (Fe) and to validate the in situ TDS data in laboratory. The collected samples were transported within 24 h of collection under refrigerated preservation to UNICEF-assisted hydrogeochemical Laboratory, Ibadan, Nigeria. Modeling of the water table and dispersion trend of ions was by Surfer 11 software.

Results and interpretations

Characterization of bedrock structures

Geology of linear features

Fracture traces were analyzed based on lineament orientation of the adjoining region in a map scale of 1:80,000 (Fig. 3),

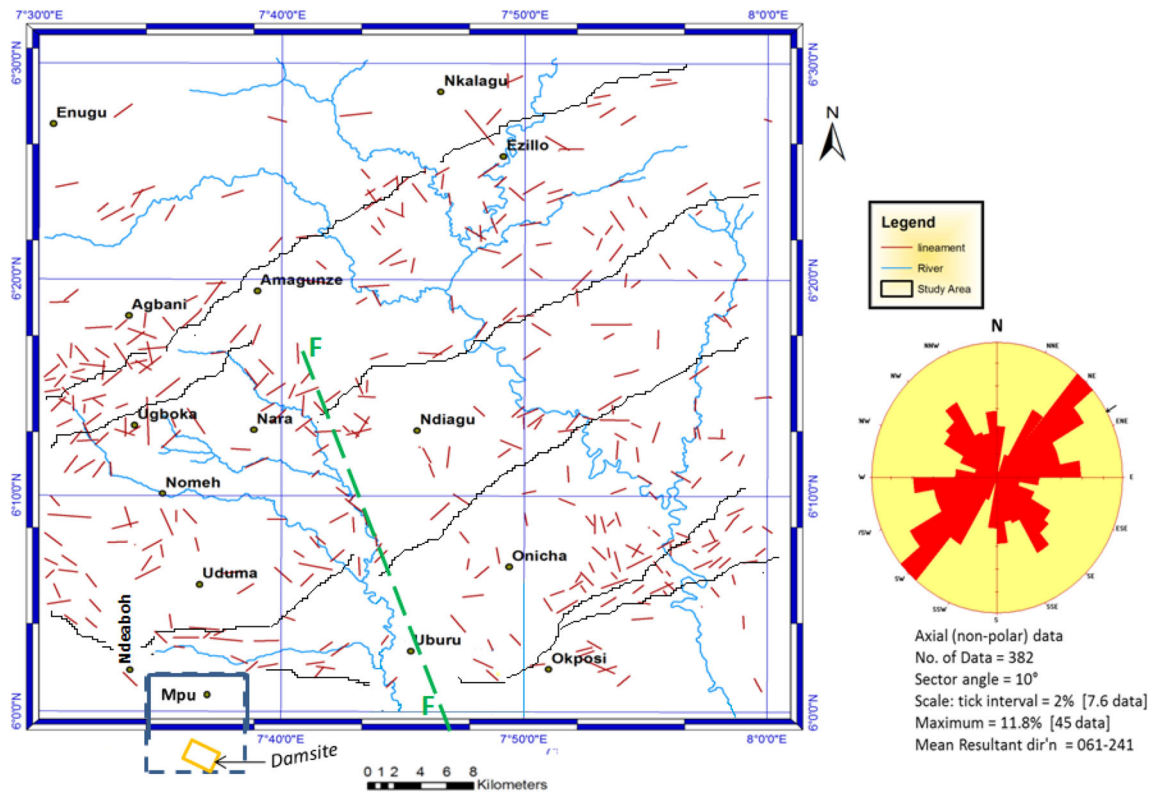


Fig. 3 Lineament map on a regional scale showing northern part of Mpu district at extreme south of Nkalagu region (sheet 302) while the dams site locates outside the map at southern part of the (Mpu) district (modified from Ukpai 2018)

hence filtered out non geological linear features (Ethan and Weikel 2008) in mean resultant $061-241^{\circ}$ direction. Ground confirmations showed that the NE-SW-oriented geologic features in the region are mainly representative of axial fractures (Ukpai et al. 2019) and conform to those delineated from cross-correlated gravity data by Onyedim (2007). As seen in Fig. 3, the fractures trend at constant sector angle of about 10° , and were generally displaced towards Western axis of the region by a NW-SE trending major fault line. Regionally, the fault node produced River Asu along the same direction. Ukpai and Okogbue (2017) had identified such node near Uburu salt Lake, about 2 km northeast of Mpu district. Therefore, it is suspected that the studied district where the dams site locates might have been affected, particularly by regional fracture sandwiched in the anticline of Asu River Group. This deduction agrees with Ukpai et al. (2019) who juxtaposed fracture traces with anticlines-synclines in stratigraphic map of lower Benue Trough, as well as Robert (2009) in Atlantic fracture zones of Benue Trough. For the fact that the syncline-anticline features extended to the dams site mean that the site was affected by geologic expressions of the linear features relating to the fault node in form of axial fractures. Therefore, geotechnical issues concerning the dams site can be linked to both regional and local defaults, from the respective lithostratigraphy and possibly, hydro-structural condition.

Lithofacies

Figure 4 presents results of forensic litho assessment around the dam, and showed major geological units underlying Mpu district as follows: Lower Cretaceous shales of Asu River Group (unit A), Upper Cretaceous shales of Ezeaku (unit B), and Awgu (unit C) Groups of Albian, Turonian, and Coniacian ages, respectively. Sandstone unit assigned to unit D and dominated Mpu Hill with some characteristics similar to Agbani Formation formed the youngest stratigraphic unit of Coniacian age in the area. Although the hill rests on Ezeaku shale (Umeji 2002), this study identified part of unit D (i.e., Agbani Formation) to overlap unit A (Asu River Group) at the extreme northeastern portion of the area (see Fig. 4). The overlapping contact has been inferred as localized unconformity, in agreement with Nwajide (2013) who noted that lithic column of Mpu Hill is separated from the underlying folded facies of southern (i.e., lower) Benue Trough by angular unconformity. Lithofacies comparisons and assessments distinguished each unit as described in Table 1. Detailed analyses are however restricted to units A and B which underlie the dam site. A local field expression of linear features in form of joint as typically seen in Appendix 2 was observed at $7^{\circ} 37' 58''$ N and $5^{\circ} 57' 45''$ E, about 500 m to the dam. The joint is azimuthing parallel to the unconforming NE-SW-oriented geologic contact along an untarred road to the dam. It is the

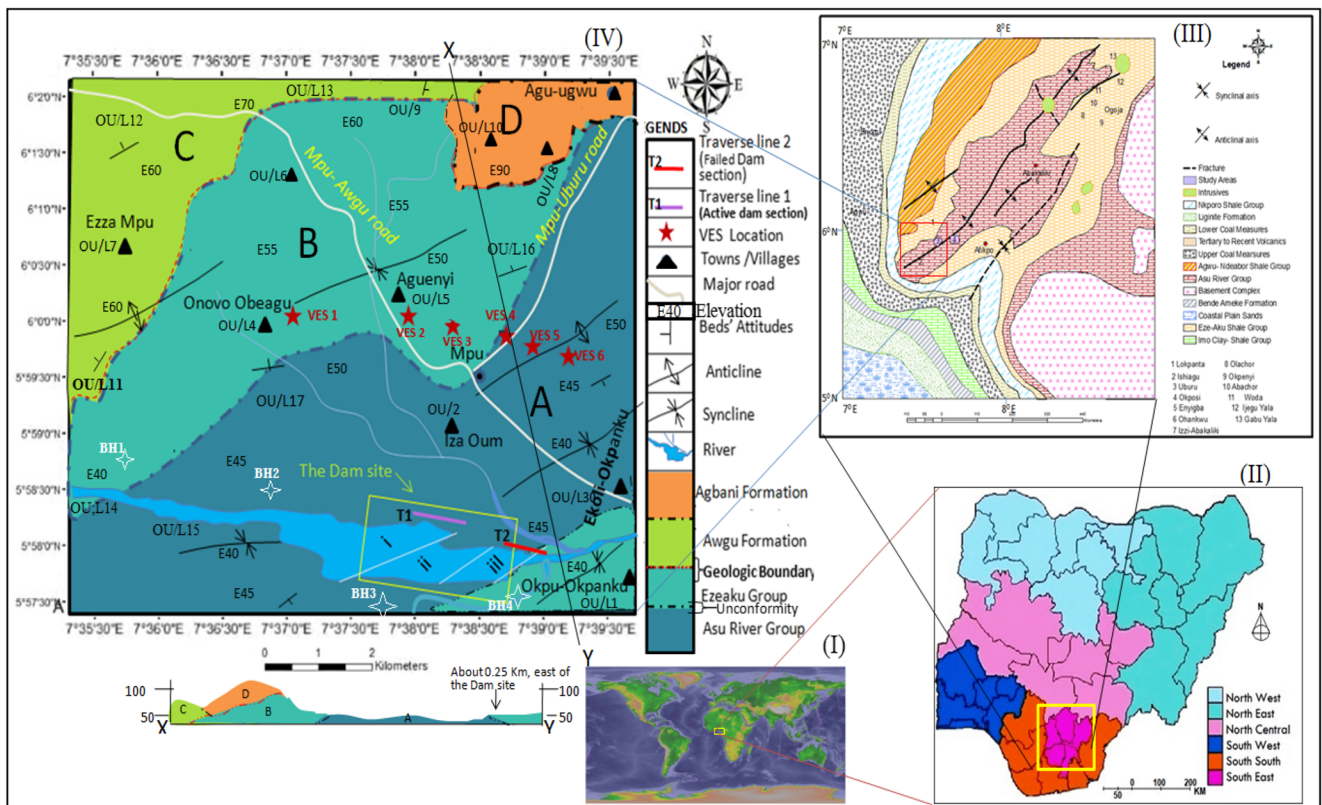


Fig. 4 Maps of (I) African-Global viewpoint, (II) Nigeria and the Southeastern portion, (III) viewpoint of the Southeastern Nigeria, and the study area (IV) showing the dam site region

field expression of a fracture trace identified towards northeast of the landscape view of the damsite (see Fig. 2). Typically, the linear features constitute structural weak zones between bedrocks (Prucha 1992; Tiren 2012) but the rock mass, mainly the Asu River Group, was manually confirmed as hard by breaking the outcrops in more than one (1) hammer blows, unlike that of Ezeaku Group that was broken in a single stroke. The Asu River Group is getting jointed with intense weathering of matrix where it has been exposed to chemical alterations or ferruginization (Fig. 5I), yet, its fresh shale occurred massively in hard flakes (Fig. 5II) but in hard seam-like formation (Fig. 5III). The fresh shale was quarried around Mpu district (Fig. 5IV) for chipping and aggregate materials, hence, would relatively be proved as indurate. However, the overlying unit B was identified as flaggy (Fig. 6I), highly fissile (Fig. 6II), slickensided (Fig. 6III) with siltstone

interbeds (Fig. 6IV), and iron-stained weakly bonded laminar, especially where it underlie units C and D conformably towards northern part of the district. This agrees with Okoro (2016) who had reported high lamination characteristic of Ezeaku Shale. The flaggy and weakly bonded laminar underscored more weak nature of bedrocks belonging to Ezeaku than the Asu River Groups. In general, these physical features were further validated by characterizing the strength vis-a-vis strength index.

Strength index of the bedrocks

Although the bedrocks at the river channel near the dam were masked by the paludal nature of the environment, however, the outcrops were identified at the river bank around upstream and downstream portions as Asu River and Ezeaku Shales.

Table 1 Litho unit descriptions

Age	Formation	Group	Lithology	Units	Description
Coniacian	Agbani	Awgu/Agbani	Sandstones	D	Poorly-moderately sorted, fine-medium grained, thick lateritic cover.
	Awgu		Shale	C	Fissile, bluish; locally ferruginized
Turonian		Eze-Aku	Shale	B	Flaggy, dark shale; highly argillaceous
Albian		Asu River	Shale	A	Indurate, bluish-dark; fairly argillaceous

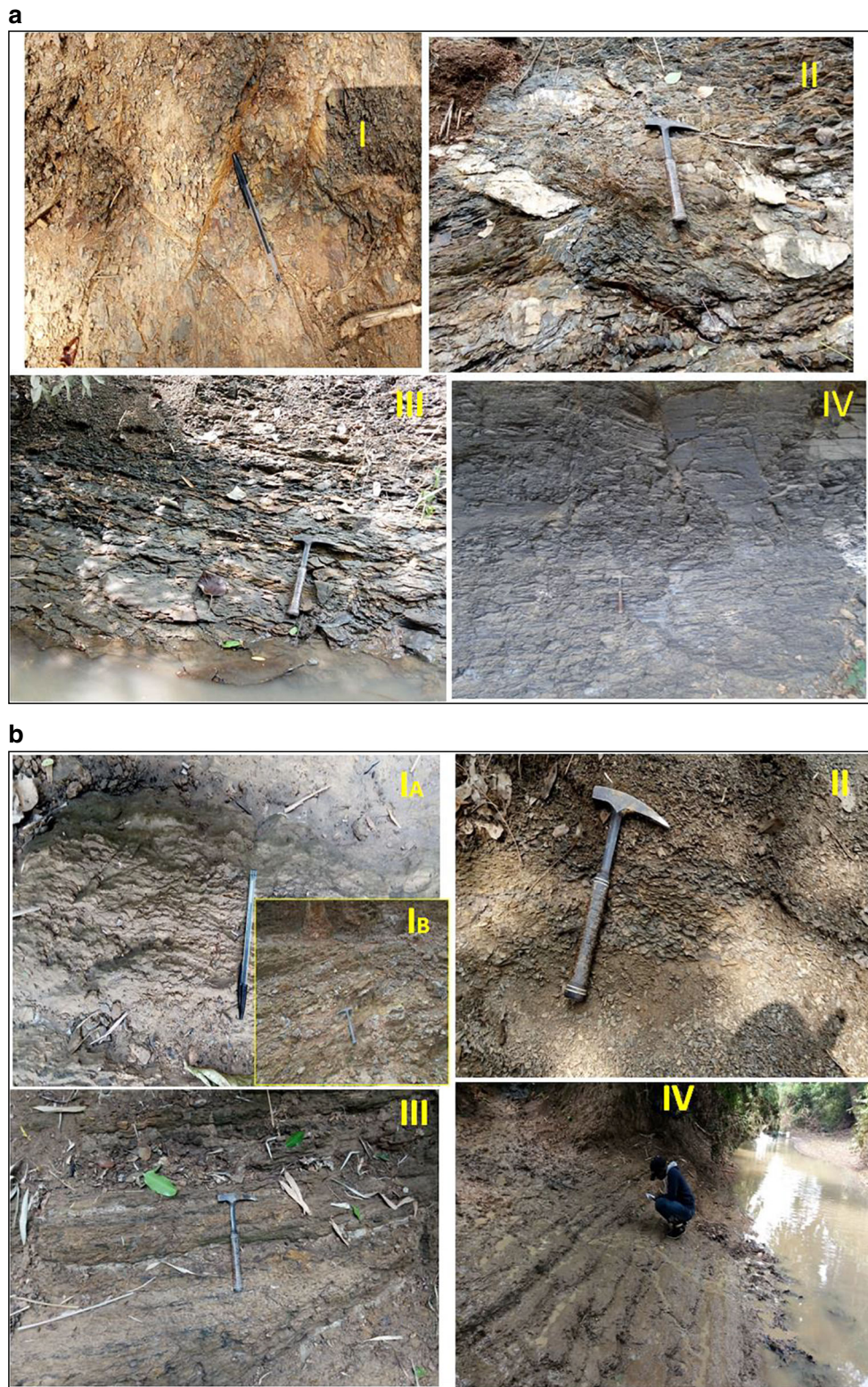


Fig. 5 a Outcrops of Asu River Shales. (I) Highly ferruginized shale in Iza Ovum (OU/L2); (II) micaceous and in hard flakes (OU/L17); (III) in hard seam-like form at upstream river bank of the dam site (around OU/L15); (IV) bluish colored at a derelict quarry pit near Okpanku Area (OU/L3). **b** Outcrops of Ezeaku Shales. (IA) Clayey, laminated, and flaggy around Aguenyi area (OU/L5); (IB) siltstone outcropping in Ezeaku Group along

traverse 2 (OU/L1) near tailwater section; (II) fissile at eastern boundary between Ezeaku and Asu River Group; (III) iron-stained, dark-gray carbonaceous, slickensided shale with siltstone lens at downstream axis of the dam site (OU/L1); (IV) slickensided with interbedded siltstone lenses at Okwa Ovum River Bank around Onovo-Obeagu

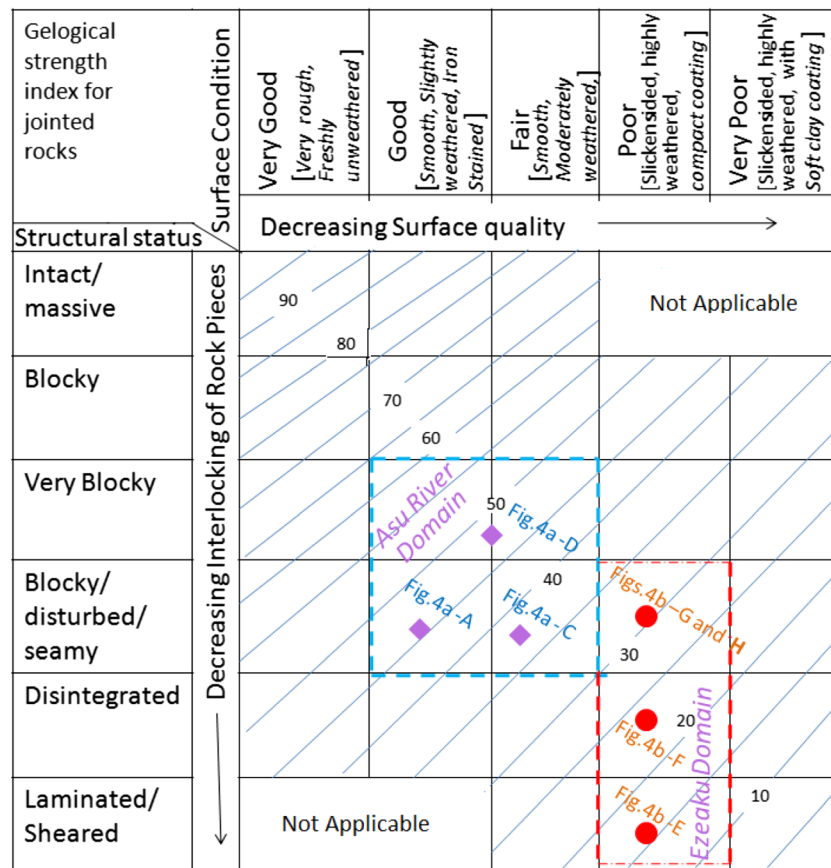


Fig. 6 Geological strength index (GSI) chart (as proposed by Marinis and Hoek 2000)

Scrutinizing the structures of the outcropped bedrocks with respect to geological strength index (GSI) chart (Hoek et al. 1995) based on block sizes and joint conditions, the GSI values ranged from 35 to 60, and 10 to 35 (Fig. 7) for Asu River Group (see Fig. 5) and Ezeaku Group (see Fig. 6), respectively. Marinis and Hoek (2000) presumed GSI ranges typical of Asu River Group as good, whereas the Ezeaku Group lies between fair and poor. The results revealed structural status vis-a-vis physical conditions at the surface.

For the fact that these bedrocks underlie the supposed zone of foundation influence, the subsurface image of the damsite was outlined for forensic assessment, particularly, to verify major cause of sagging at the tail water axis (see Fig. 1c).

Hydrogeophysical character of litho units

Geoelectrical image of the foundation zone

Geoelectric models (Fig. 8a and c) delineated configurations of the underlying bedrocks around the foundation zone. Observably, the dam stretched across the geologic contact (or gap) between Asu River Group which extended down-slope from the axial Abakaliki Anticlinorium, and Ezeaku Group which prograded from Afikpo sub-basin. As seen in

the models, typical rock resistivities (Loke 1999) deduced three major geoelectric units (Figs. 8b and d). Ranges of resistivities from 34.7 to 90.8 Ohm m were interpreted as weathered/ferruginized shale (see Fig. 5I) with patches of iron residues (see Fig. 6I, II, III, IV); from 4.2 to 7.5 Ohm m was interpreted as clayey layer which marked the basal limit of weathered sedimentary subgrades; and from 1670.3 to 4538.2 Ohm m as the underlying fresh bedrocks (compare [Fig. 8a and b with 8c and d]). According to Lyons and Van deCamp (1980), bedrocks reflect elevated resistivities, possibly relating to induration (i.e., hardness). Inferred depths to the bedrocks varied, but with the minimum of about 10 m (see Fig. 8). The depth increased infinitely where the Asu River Group prograded indefinitely into subsurface, particularly towards the end of traverse 1, about a distance of 240 m away from the initial line of the traverse (see Fig. 8a and b). Axis of the sedimentary progradation in the field (by latitude and longitude) was located on geologic map (see Fig. 4IV) as a boundary where Asu River Group dipped into Ezeaku Group.

Inferred seepage paths

Information from Fig. 8c guided in macroscopic tracing of the clay unit to its outcrops along traverse 2, about the distance of 340 m from the downstream tail water section. It was identified

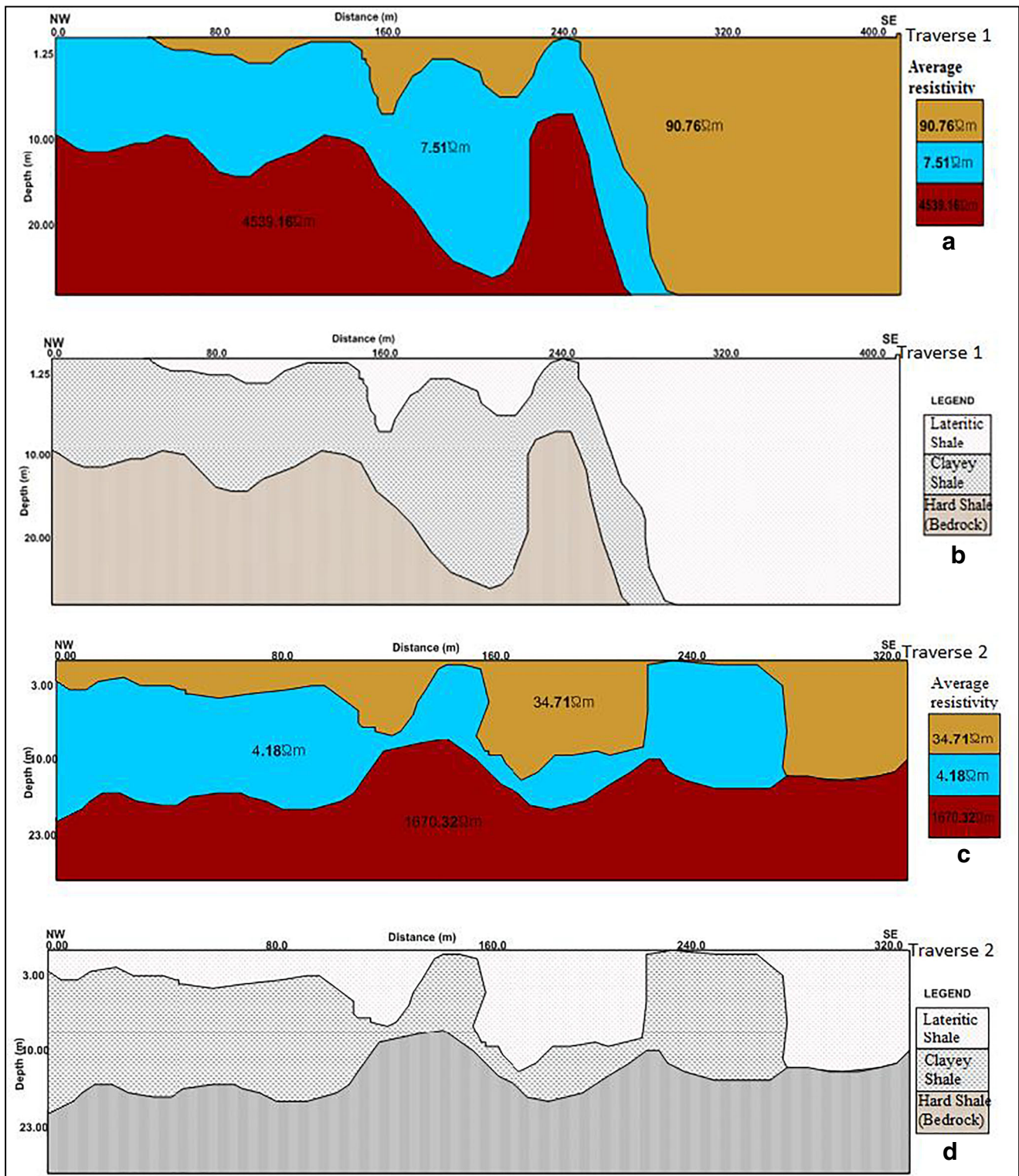


Fig. 7 Geo-models. a Resistivity equivalent of (b) geologic formation in Asu River Group; (c) resistivity equivalent of (d) geologic formation in Ezeaku Group

that the layer earlier interpreted as clay is a mixed argillaceous unit that comprised siltstones (see Fig. 6IB). Furthermore, results of the 2D VES-IP (see Fig. 9) showed pseudosections which delineated discrete low chargeabilities with deeply dark

blue band (Fig. 9A2) coinciding with dark blue band for extreme low resistivity anomalies (Fig. 9A1) along the geoelectric pathway earlier deciphered and validated as silty/clayey unit. By implication, the extremely low resistivity (dark blue)

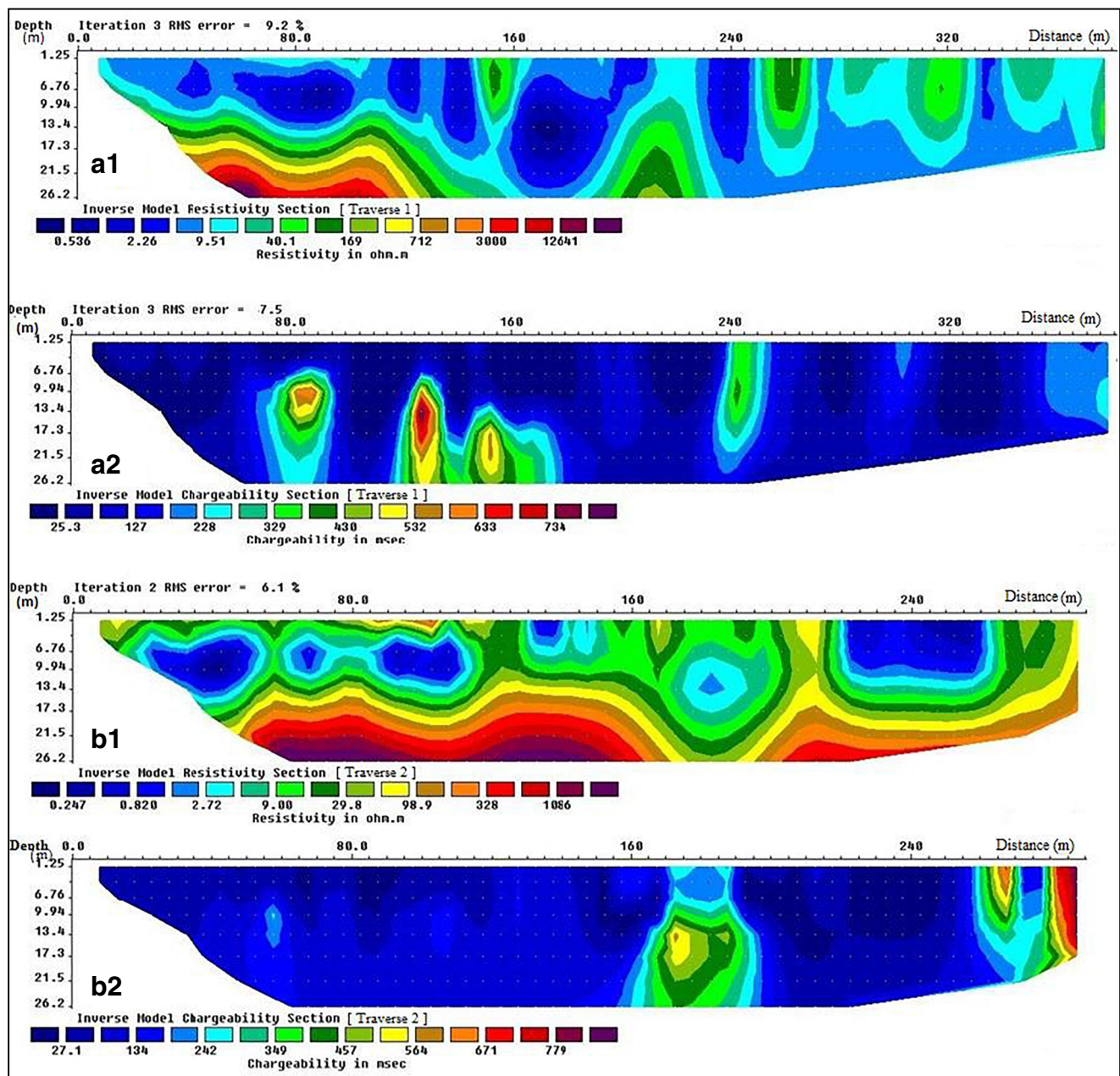


Fig. 8 Tomographs. (A1) Apparent resistivity pseudosection for traverse line 1. (A2) Apparent chargeability pseudosection for traverse line 1. (B1) Apparent resistivity pseudosection for traverse line 2. (B2) Apparent chargeability pseudosection for traverse line 2

sandwiched within blue background of low resistivity (Figs. 9A1 and B1) signified pore water mounds (i.e., the dark blue) confined within the clay/siltstone layer (represented in blue band). According to Gance et al. (2015), argillaceous units like clay/silt reflect low resistivity, whereas Rehman et al. (2016) reported that the argillites reflect high/moderate chargeability. Analogically, clay minerals reflect low resistivity, as well high or even moderate chargeability. As Ukpai and Okogbue (2017) had noted that very low resistivity is a sign of pore water concentrated with chemicals, mainly salt, it is safe to deduce that the mixed clay/silt layer infused pore water to the foundation of the dam.

It is important to note that high resistivities in Fig. 9A1 and B1 from 169 to 1086 Ω m portrayed the bedrocks with relative discrete high chargeabilities in Fig. 9A2 along traverse 1 as similarly seen in Fig. 8, but the bedrocks reflected low chargeability signal along traverse 2 (see Fig. 9A2 and B2), signifying that bedrock of Ezeaku Group is highly argillaceous. However, high chargeability anomaly is observed at the distance of about 200 m, near the tail water axis along traverse 2, and coincided with low resistivity anomaly at same distance (compare Fig. 9B1 and B2), hence, indicated confined pore water, possibly concentrated with dissolved solutes. Moreso, at about 240 m along traverse 1, a nodule-like

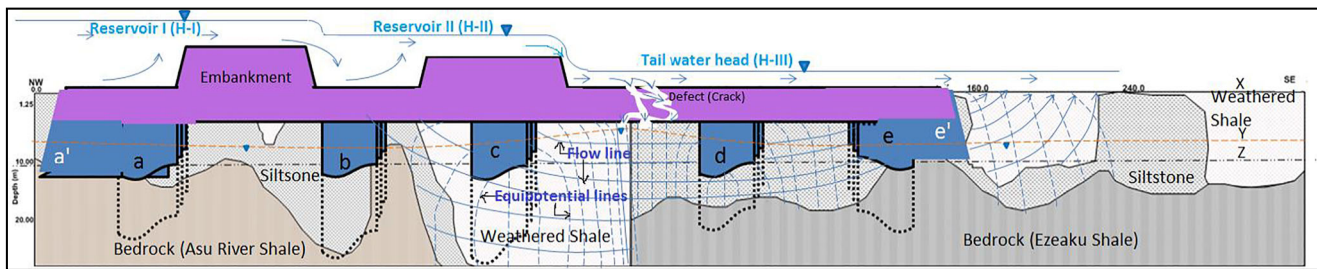


Fig. 9 Schematic representation of geologic and hydrogeologic conditions at the dam site. **a, b, c, d,** and **e** represent piled foundations, and **(a', e')** represent abutments, and **x, y,** and **z** represent ground surface, water table, and initial depth to rock heads, respectively

anomaly was identified and protruded from top of the section. This anomaly reflected low resistivity and high chargeability (compare Fig. 9A1 and A2) and was inferred as plume concentrated dissolved solutes that perhaps advected from the water reservoir through the sagging (crack) defect at the tail water axis. Similarly, from points 260 to 440 m along traverse 1, isolated noddle-like anomalies also aligned vertically from top of the pseudosection. These particular discrete anomalies reflect moderate-high resistivity between 40.1 and 169 Ω m but low chargeabilities, and were inferred as traces (trails) of iron residues. Based on the assertion of Berry et al. (2012) who noted that soil-hematite bodies reflect high resistivity and low chargeability, it means that chemicals leak into the foundation zone, especially as most outcrops are banded with iron materials (see Figs. 5I and 6). Justifiably, the concentrated chemicals confined in sediments underlying the dam can be related to ions (or dissolve solutes) flushed by surface flow and seeped into the subsurface through some exposed sandy shale (see Fig. 6II) or silty/clayey sand (see Fig. 5IB) that formed aquitards into the dam foundation.

Confined moisture content

Apart from distinguishing bedrocks of Asu River Group and Ezeaku Group with five (5) and four (4) geoelectric units, respectively, via 1D resistivity anomalies (Table 2), although generally resolved in 2D resistivity (see Fig. 8a and c) to three (3) layers, the 1D discriminated depths to water table by the initial warping of apparent resistivity curves (in red). The inferred depths to water table ranged from 5.0 to 7.5 m (see Table 2), but could not correlate significantly with ground confirmations of static water levels observed in cored holes (Table 3). This discrepancy may be due to shallower depth to saturated zone at boreholes (BH) near the river bank than the areas of the VES locations farther away from the bank. Comparing depths with water table (Table 3) with depths to bedrocks (Table 4), or even those inferred from VES (see Table 2), the bedrocks lie beneath phreatic surface. Meanwhile, the water table lies above the aquitards, hence, can absorb and store sufficient water (Rajapakse 2016) for regional flow (Todd 1980) by means of seepages (Fetter 2007). Around the studied dam, the seepage was intercepted

where the aquitards intersect the boundary between bedrocks of the geologic groups underlying the dam. Due to the downdip orientation of the bedrocks towards the boundary point, the seeping water was topographically confined, resulting in pore water mounding, particularly around piles {c} and {d} (Fig. 10) as identified at adjacent BH 3 (Fig. 11a and b). The seepage was recharged at upstream areas, about few distances away from the dam as typically depicted by decreased hydraulic head with depth at BH 2, while height of the hydraulic head towards or above the water table near BH3 (see Fig. 11b) signified the discharge into the dam foundation. This analogy agrees with Chilton (1996) who stated that decrease of hydraulic head with depth and downward net saturated flow away from the water table indicates recharge area, whereas increasing head and configuration of net saturated flow upwards and towards, the water table shows discharging groundwater spot. Marinos and Hoek (2001) highlighted that moisture content influences strength and deformity of shale as a sedimentary rock.

Hydrogeochemical status of foundation zone

Comparison of Fig. 11a and b with 11c and d showed that both recharge and discharge ends of pore water seepage corresponded with respective discharge and recharge spots of total dissolved solutes (TDS). By this fact, it is believed that the dissolved solutes evolved from weathered outcrops (see Fig. 5 and 6) via advection process. Density of the pore water can be slightly raised by salinity (Oude Essink 2001) inflicted by concentration of the TDS (see Table 3). Difference between the TDS measured in situ (TDS1) and laboratory results (TDS2) is less/or equals to 10 mg/l in favor of those measured in situ, except in BH3. Both concentrations of the TDS in BH3 nearest to the dam are higher than those from the adjacent boreholes (BH), hence, signified concentration anomaly beneath the foundation (Fig. 11c and d). Apart from effects of chemical processes relating to dissolved solutes on geotechnical quality of the rock heads, confined TDS concentration of this nature can cause compression of pore water to exert pressure (H_p) locally; and with the increasing energy head due to continuous seepages into the foundation, vertical uplift pressure (P_u) thus aggravates, following Eq. 9:

Table 2 Results of the 1-D resistivity survey

VES no	Location names	Depth to layer 1 (m)	Depth to layer 2 (m)	Depth to layer 3(m)	Depth to layer 4(m)	Overburden thickness (m)	1 (Ohm m)	2 (Ohm m)	3 (Ohm m)	4 (Ohm m)	5 (Ohm m)	Formation	Inferred water table depth
VES 1	Onovo Obaagu	0.013	0.38	1.23	2.91	Lower limit not yet detected	3.13	164	0.048	6.04	0.018	B	7.5
VES 2	Aguenyi	0.61	5.89	96.9	-		35.5	0.21	0.012	2.6×10^{-5}	-	B	5.0
VES 3	Mpu Junction	0.61	0.96	13.4	-		35.0	0.43	0.050	6.9×10^{-3}	-	B	5.0
VES 4	Mpu-Uburu Rd	1.08	1.37	3.03	-		0.88	0.01	0.257	6.3×10^{-3}	-	AB	5.0
VES 5	Iza 1	0.93	5.25	41.3	69.0	69.0	13.3	1.05	3.253	8.8×10^{-4}	0.304	A	5.2
VES 6	Iza2(ByAniriLG Hqtrs)	0.61	5.9	96.7	194.0	194.0	36.3	0.21	1.12	2.9×10^{-5}	0.304	A	5.9
Mean (average)													

Values in italics are layer resistivities with corresponding depths indicating the water table between depths of higher resistivities A, Asu River Group; B, Ezeaku Group; AB, boundary between A and B

Table 3 Results of ground-validated groundwater level, geochemical analysis, and other hydraulic parameters

Location Code	Coordinates				Borehole data								Hydrogeochemical data			
	Latitude (Norths)	Longitude (Easts)	E_L (m)	TDD (m)	E_h (m)	Depth to SWL	H_h (m)	H_p (m)	P_u MPa	TDS1 (mg/l)	TDS2 (mg/l)	EC ($\mu\text{S cm}^{-1}$)	pH	Fe(mg/l)		
BH 1	5°58' 50"	7° 35' 45"	45	12.7	32.3	4.5	40.5	8.2	0.08	144.0	138.6	255.0	7.3	0.318.		
BH 2	5°58' 30"	7° 36' 36"	44	11.2	32.8	5.0	39.0	6.2	0.06	115.0	106.5	194.0	7.6	0.263		
BH 3	5°57' 30"	7° 37' 45"	43	11.8	31.2	2.5	40.5	9.0	0.09	198.0	203.0	372.0	7.1	0.522		
BH 4	5°57' 35"	7° 38' 50"	43	13.4	29.6	3.0	40.0	10.4	0.102	165.0	160.0	388.0	6.7	0.704		
River sample (collected at heel head [H-II] portion of the water reservoir)																
										100.0	98.0	179.0	8.0	0.320		

TDS1 and TSD2 are in situ and laboratory results for total dissolved solids (TDS), respectively

BH borehole, E_L elevation from mean sea level to ground surface, E_h elevation head, P_u uplift pressure, TDD total drilled depth, SWL static water level (in meters), i_{exit} exit gradient, H_h hydraulic head (or total head)

$$P_u = H_p * \rho_w * \bar{g} \tag{9}$$

where ρ_w and \bar{g} are density of water and gravitational field strength, respectively. Since assumption of 100% uplift pressure signifies leakages through cracks on dam embankment (Don et al. 2009), the uplift force is strongly exerted in this case, especially as factors (or variables) that intensified the parameter into the densed pressure head (H_p) exist (compare Eqs. 9, 10, and 11). Fixing variables of Eq. (10) in Eq. (9) with values in Table 3, as well as taking standards of ρ_w and \bar{g} as 1000 kg/m^3 and 9.8 m/s^2 , respectively, $8.036 \times 10^4 \text{ kg/m s}^2$ (or 0.08 MPa), $6.076 \times 10^4 \text{ kg/m s}^2$ (i.e., 0.06 MPa), $8.82 \times 10^4 \text{ kg/m s}^2$ (or 0.09 MPa), and $1.019 \times 10^5 \text{ kg m}^{-1} \text{ s}^{-2}$ (0.1 MPa) represent the P_u from upstream to downstream areas, comprising the respective BH1, BH2, BH3, and BH4. Thus, elevated amount of P_u at BH 3 indicates the pressure anomaly at the dam base nearest to the shear zone between piles **c** and **d** (see Fig. 10), and the nature of increase towards the toe axis in BH 4 confirmed the effect of the unconfined leakage as major contributing factor.

$$H_p = H_h - E_h \tag{10}$$

by which;

$$E_h = E_L - TDD \tag{11}$$

while parameters are defined in Table 3.

Site-specific geotechnical assessment

Rockhead qualities

Apart from investigating in situ qualities of the bedrocks by rock quality designation (RQD) and other parameters in rock mass rating (RMR), the information about varied depths to the rockheads underlying the dam was confirmed in the coring operation (Table 4). A sound sample of length (L) less than 1 cm was considered as $L = 0$ (Fig. 12), and qualitatively unfit for use in determining the RQD shown in Eq. (12), as:

$$RQD = \frac{\sum \text{Sound Core Pieces} > 1 \text{ cm}}{\text{Total core run length}} * 100 \tag{12}$$

The data from Fig. 11 was subjected to Eq. (12), and results showed RQD as 65.5%, 86%, 77%, and 44% for BH1, BH2, BH3, and BH4, respectively (Table 5). Thus, the RQD ranged from 44 to 65.5% for Ezeaku shale and 77 to 86% for shales of Asu River Group. Correlating the results with RQD standards specified for hard shales by Look (2007) and Briaud (2013), the Asu River shale was adjudged good while Ezeaku spanned from fair to poor qualities. Further validation from integrated parameters in RMR (see Eq. 1) presented values as 54 and

Table 4 Results of compressive strength

		Coordinates of Sampled Location										Date: 24 -04 -2019				
		Lat: 6° 20' 30"-5° 57' 30"														
		Long: 7° 35' 30"-7° 35' 30"														
BH No	Depth (m) to bedrock	q_c (i.e., UCS) (MPa)	ϕ (°)	$\alpha = (45 + 1/2\phi)$	N_ϕ	q_{ult} (MPa)	FS	q_{lat} (MPa)	D (mm)	L (mm)	P (kN)	A = L x D _e (mm ²)	D _e (mm)	D _e ² (mm ²)	I _s (MPa)	I _{s50} (MPa)
		Measured	Predicted													
BH1	7.2	20.51	20.46	13	51.5	1.58	52.9	2.5	21	59	4.23	5402	74.1	5491	0.77	0.93
BH2	6.5	21.47	21.34	14	52	1.64	56.68	2.5	23	61	4.6	5498	76.3	5822	0.79	0.97
BH3	8.4	20.77	20.68	18	54	1.89	60.02	2.5	24	74	5.8	807	91.1	8299	0.70	0.94
BH4	8.4	19.23	19.14	18	54	1.89	55.57	2.5	22	65	5.2	8554	89.1	7944	0.65	0.87
Mean		20.50	20.41													0.73

UCS was predicted from (axial) point load test, but measured directly via compression test

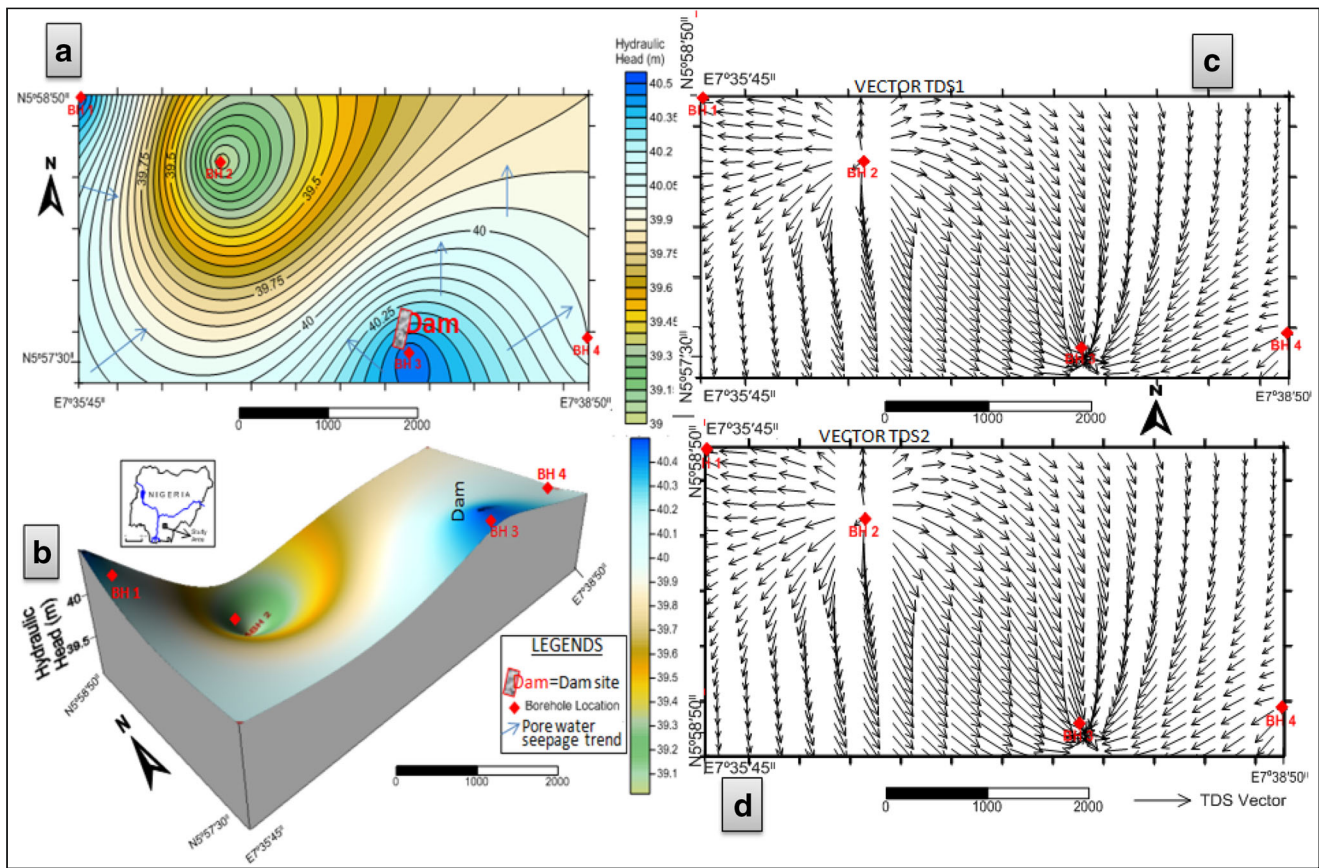


Fig. 10 Maps showing (a) hydraulic head in 2D depicting seepage trend, (b) surface configurations of hydraulic head in 3D, (c) dispersion vectors for TDS 1, and (d) dispersion vectors for TDS 2

47.5 for Asu River and Ezeaku Groups, respectively (see Table 5) but generalized the qualities of both shales to fair

category. This generalization is based on the classification of RMR within range (from 41 to 60) as fair (Indian Standard 1987).

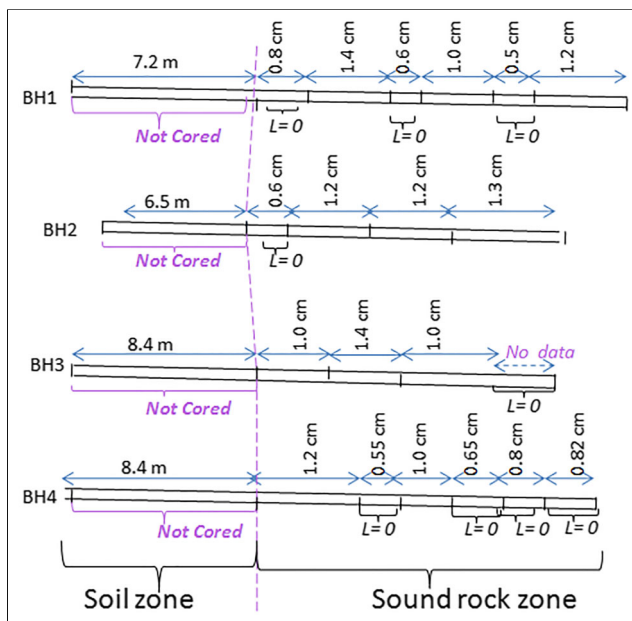


Fig. 11 Measured molds of the core sample across the Boreholes from surfacial (soil) zone to subsurfacial (fresh rock) zone

Shear and compressive strengths

Seeing that most parts of the rock heads (bedrock columns) are somewhat unsound (see Fig. 12; Appendix 3b), ultimate bearing capacity (q_{ult}), in addition to allowable bearing capacity (see Eqs. (2) and (5)), was determined (see Appendix 4 in ESM) to check capacities for end bearing piles. Table 4 shows results of compressive strength and shear strength tests as follows: uniaxial compressive strength, UCS ranged from 19.2 to 21.5 MPa with negligible difference of about 0.1 MPa greater than predicted values, ultimate bearing capacity (q_{ult}) from 52.9 to 60.1 MPa (i.e., 539.4 to 612.8 kg/cm²), and safe or allowable bearing capacity (q_{al}) from 21 to 24 MPa (or 214.1 to 244.7 kg/cm²). Close comparison of the data in Fig. 12a showed that the UCS is linearly related with point load strength index (I_{S50}), hence indicate that one can be predicted from another as shown in Eq. (8). Precision of the measured UCS was indicated in the predicted values as both showed linear equality (Fig. 12b). The determined

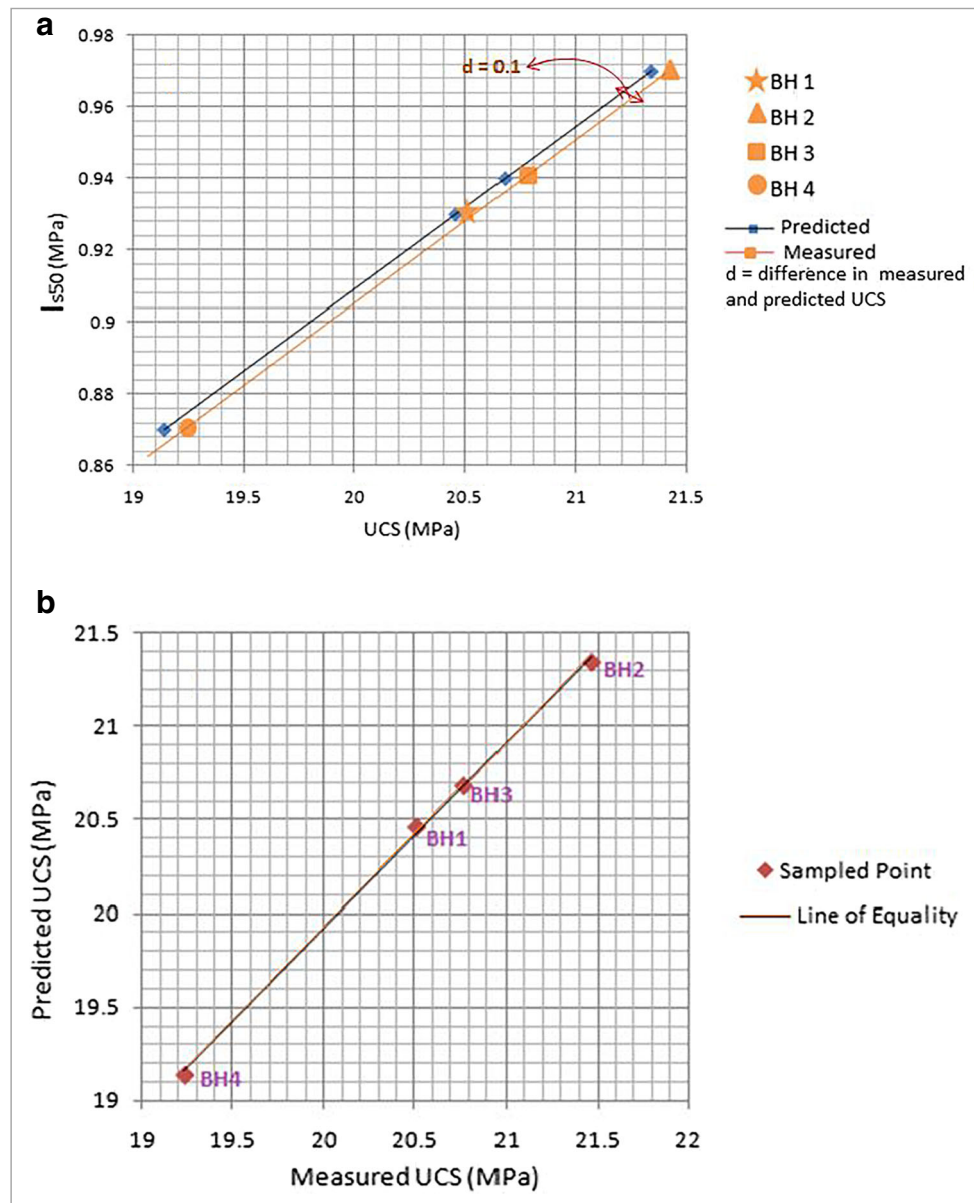


Fig. 12 Graphs showing linear relationship between (a) point load index (I_{s50}) and UCS, (b) measured and predicted uniaxial compressive strength (UCS)

UCS is higher than the 18 MPa standard highlighted by Kawasaki et al. (2002). Relatively, elevated values of q_{ult} signified that the bedrocks satisfy ultimate limit (i.e., state of safety criterion) to bear load of the dam without being stressed to probable failure. The estimated q_{al} values of the end bearing bedrocks surpassed the 25.5 kg/cm^2 presumed as threshold limit by Indian Standard, IS (1987), for net allowable bearing pressure in typical hard shales. Linearly, q_{ult} and q_{al} are parallel, possibly due to common relationship with factor of safety (FS) as shown in Eq. (5). The FS was selected to about 2.5 justified as global factor of safety for deep foundation (Briaud 2013) or for normal control in permanent foundation (BNBC 2012).

General discussion

Direct contact between the Asu River Group and Agbani Sandstones around Mpu Hill, as well as between the Asu River and Ezeaku Groups, means that there are gaps of non-deposition or that the study area was seriously affected by paleo erosions. Therefore, the area is a terrane with overlapping heterogeneous rocks in crosswise variation of wide geologic ages. Combination of these rocks of varied properties imposes complex geotechnical engineering problem (Goodman 1993). According to Martin et al. (2017), heterogeneity of sediments affects ground behavior against geotechnical conditions. However, the indurate nature of fresh shale

Table 5 Results of rock quality parameters and rock mass rating

Parameter	Geological formation/group						Rating based on Waltham (1994) on core data only	
	Asu River (unit A)			Ezeaku (unit B)				
	BH 2	BH 3	Outcrop	BH1	BH4	Outcrop		
Color	Bluish	Bluish	Bluish dark	Dark	Dark	Dark gray	-	
G. water condition	Damped	Damped	Nil	Damped	Damped	Nil	Damping = 10	
Fracture	Weathering	Fresh	Fresh	Weathered/blocky	Fresh	Fresh	Weathered/flaggy	
	Spacing	> 60 mm	> 60 mm	-	> 60 mm	> 60 mm	-	60 to 200 mm = 8
	Orientation	Isotropic	Isotropic	Isotropic	Isotropic	Isotropic	Isotropic	Isotropic = fair = -7
	Condition	Tight	Tight	A bit weathered	Tight	Tight	Weathered	Open < 1 mm = 25
RQD (%):	86	77	-	65.5	44	-	Unit A = 17 Unit B = 10.5	
	Unit A: if within 75–90% = 17			Unit B: 25–50% = 8; 50–75% = 13				
UCS (MPa)	21.5	20.8	-	20.5	19.2	-	1 to 25 MPa = 1	
Hardness	-	-	No dusty rubbles	-	-	Dusty rubbles	by Knife Scratch	
Strength	-	-	Few blows	-	-	One (1) blow only	by Hammer blow	
Rock mass rating (RMR)	10 + 8 + (-7) + 25 + 17 + 1 = 54			10 + 8 + (-7) + 25 + 10.5 + 1 = 47.5			Unit A = 54 Unit B = 47.5	

Spacing was assumed via visual impression

Isotropic, directional; *G.water*, groundwater

of Asu River Group signified that the bedrock mass is somewhat more suitable than Ezeaku Group to bear stresses from such a heavy structure like dam.

Resistivities of the bearing surfaces however differed from 1670 Ohm m in traverse 2 mainly within Ezeaku Group to 4539 Ohm m in traverse 1 covering Asu River Group (compare Fig. 8a and c, b and d). This has further signified harder nature and better quality of underlying rockmass belonging to Asu River than the Ezeaku Group. Thus, imbalance due to the differential rockhead qualities at boundary between the two sedimentary groups would be attributed to onset of instability under the dam. Moreso, an inferred layer, comprising silty/clayey sand, marks top of the rockheads, hence formed aquitard which links the outcrops adjacent the damsite and streamlined seepage of water from overland flow system to the unstable (weak) geologic boundary underlying the dam. Movement of the solutes along with seepage caused the concentration of the TDS around BH3 (see Fig. 11c and d) directly at foundation zone, and had been suspected to enhance density of the pore water by instilling salinity to the locally confined pore water mound beneath the dam (see Fig. 11a and b).

Such hydrological impasse may not have only injected chemical weathering on the foundation bearing through the concentrated TDS but possibly raised uplift pressure vis-a-vis bumping up of water density under the dam. This is strongly suspected to result in the sagging (failure mode) at the tail water head (see Fig. 1c). The sagging spot was traced to the geologic boundary in Fig. 4IV. Varied depths to rockhead as seen in Fig. 8 can be related to deterioration of its top limit by

the chemical weathering. Hence, generated ambiguity led to inappropriate footing of some foundation pile on weathered portion (subgrades) which intermingled between the bedrocks. For this reason, it is required that the foundation must be piled deeper beyond the subgrades into the bedrock, at least greater than 20 m as projected in Fig. 10. Fresh bedrock at such depth could form safe bearing surface against near surface processes relating to above limit concentration of dissolved product of chemical weathering like dissolved Fe (see Table 3).

Presently, as the foundations are just ≤ 10 m deep (see Fig. 10), the dam weight rests on the rock head near the surface where it has been gradually weakened by reaction of dissolved iron to form hematite (Ukpai et al. 2017), as shown in Eq. (13), thus (Roberge 2006):



Reaction in Eqs. (13) and (14) is possible because the pore water (solution) is more alkaline by which oxidation of Fe takes place. Evidence of iron oxides can be explained by brownish and red colors as mainly seen in Fig. 5I and signifies rusts (Duarte et al. 2018) such as the product of Eq. 13, i.e., Fe_2O_3 (hematite or iron [III] oxide) being a common feature of alkaline corrosion of steel (Bignold 2003). This corrosion was mainly ignited because Fe_2O_3 is water adsorption medium (Kvamme et al. 2012), although could get hydrated to $2\text{Fe}(\text{OH})_3$ (see Eq. (14)) and precipitated out of solution at higher

pH (Freeze and Cherry 1979), hence would have accounted for slighter concentrations in BH 1, 2, and 3 than BH 4 (see Table 3). But rusts easily form acid anhydrides (Chipperfield 2003) like ferric sulfate $[\text{Fe}_2(\text{SO}_4)_3]$ which made the movement of the concentrated iron material easier (Scholz 2006) from run off into subsurface foundation zone where it was suspected to undergo further reaction. Such typical acid-rock drainage (ARD) was strongly believed to be influencing the pH of the mounding pore water around the dam foundation at BH 3 (see Fig. 11a and b) towards acidity (see Table 3). According to Ga'l (2000), acidic water dissolves rock minerals. Thus, undulating nature of the bearing surfaces (see Fig. 8) has been attributed to weakening of the end bearing (or rock heads) fabrics because of its vulnerability to induced chemical weathering. The weathering process affected geotechnical qualities of the bedrocks.

Generally, $I_{S(50)} < 1.0$ MPa; therefore, the rock masses were rated from UCS in RMR (Bieniawski 1989). The UCS showed mean strength of about 20.5 MPa for the shales (see Table 4) indicating intact and blocky wet bedrocks at about the depth of ≥ 10 m except at the unconforming boundary between unit A and B where the subgrades prograded deep into subsurface. Another prime RMR parameter like RQD showed good qualities of the fresh bedrock masses for Asu River Group (i.e., unit A), and from fair to poor qualities for shales of Ezeaku Group (unit B). However, the overall RMR certified strengths of the entire rock masses underlying the dam site as fair. According to Waltham (1994), strength of bedrocks is certifiable with $I_{S50} \geq 1.0$ MPa and UCS ≥ 20 MPa. Although the mean I_{S50} is about 0.93 MPa (see Table 4) and less than standard limit, the UCS being greater than the minimum specification balances the strength status of the rock mass to fair condition. It means that quality of concrete for grouting the settling portion, encasement of steel piles, and other maintenance services should not be less than 20 MPa of UCS. Typically, allowable bearing capacity (q_{al}) for residual deposits such as hard shale was presumed 880 kPa by Sitharam (2019) and 1500 kPa if dry and 3000 kPa for fractured rocks (Look 2007); all are significantly less than 21,000 kPa (or 21 MPa) being the minimum estimated at BH1 (see Table 4). This indicates that the bearing surface is so stable to bear the weight of the dam if factors that would trigger geotechnical conditions were absent.

It implies that failure modes within the dam were orchestrated by physical condition of the damsite (Mansuri et al. 2014) like the undulated nature of the bearing surfaces due to chemical degradation of the near surface rock heads, as well as the confinement of the seeped water under the dam through a composite aquitard. It is believed thus that at the onset, the aquitards streamlined seepages from its outcrops at upstream vicinities of the dam into the massively weathered boundary zone, between piles c and d (see Fig. 10). Consequently, the hydraulic head was locally heightened at BH 3 nearest to the

dam foundation (see Fig. 11a and b), hence, compromised stability of the dam by developing the crack-forming defect on portion of the embankment where the dam weight rested directly on weathered rock heads. This heaved the foundation columns, resulting in the settling cracks at the tail water axis. Thus, with increasing volume of confined pore water due to vigorous inflow of water from the reservoir into the foundation through the vertical crack, and with increasing pore water mass due to the concentrating salinity from chemical reactions, uplift pressure (P_u) is strongly induced as locally observed at the base of the dam between piles c and d. Seeing that the P_u was built up into the downstream seepage exit around the toe axis (at BH4) against typical setting by which it should have decreased towards the downstream means that the pressure will eventually inflate the dam weight and jeopardize the overall stability.

If weight of the dam (D_w) is calculated as density of concrete (C_d) multiplied by product of dam base thickness (B) and gravitational field strength (\bar{g}), as given in Eq. (15):

$$D_w(\text{Mpa}) = C_d(\text{kg/m}^3) * B(\text{m}) * \bar{g}(\text{m/s}^2) \quad (15)$$

Then, the dam should be designed such that the uplift pressure (P_u) is steadily less than the self-weight (D_w). Accordingly, the size of B should be very sufficient with adequate amount of C_d , so that:

$$P_u(\text{MPa}) < D_w(\text{MPa}) \quad (16)$$

But in this study, the reverse of Eq. (16) is the case as suspected at the downstream portion of the dam foundation (defected portion) where the elevating P_u coincided with the failing portion. At this portion (i.e., columns c and d), the hydraulic gradient (i) was raised such that equipotential lines were concentrated (see Fig. 10). These columns are vulnerable to instability due to combined stresses exerted by hydraulic gradients from (1) lateral seepage through the aquitards, (2) upward movement of the mounded pore water (see Fig. 11b), and (3) the vigorous downward leakages into the dam foundation. Therefore, the hydraulic gradients (i) appeared to tend towards exit gradient (i_{exit}) at critical condition (i_{cri}), consequent upon which $D_w \approx P_u$ by which the dam submerges.

According to United State Department of Interior, Bureau on Reclamation (USBR 2014), the gradient can become critical when the value increased at least to a unit (i.e., one [1]). Presumably, the dam would remain stable for $i_{exit} < 1.0$; therefore, the factor of safety (FS) should be established at $FS \geq 2.5$ to check the i_{cri} with respect to i_{exit} using Eq. (17), thus:

$$i_{exit} = i_{cri} / FS \quad (17)$$

According to Coduto (1994), as well as BNBC (2012), bearing capacity can properly withstand failures by designing

piles to minimum $FS \geq 2.0$. Yet, consideration should be based on traditional stress design against failure which relies on FS with respect to q_{ult} and q_{al} for which (Zhang 2004):

$$q_{ult}/FS \geq q_{al} \quad (18)$$

During rehabilitation measures or in designing a new dam, prerequisite should be taken on the basis of Eqs. (15), (16), (17), and (18). Grouting leakage zone using quality cement of $UCS \geq 20$ MPa can knit with the UCS of the bedrocks. Particularly, jet-grouted diaphragm cut-off wall can water-tighten as much as possible, and in case of constructing new dams, it should be emplaced after wall construction for quality control against defect (Pan and Fu 2020). Although defects in cut-off walls were regularly reported (Tan and Lu 2017; Hwang et al. 2016), attention should be devoted to penetrate the cut-off very well into the leakage axis being treated to prevent deviations. Moreso, further precautions should be keenly taken to avoid variations in the dimensions (lengths or widths) of the diaphragm columns in order to close up the targeted seepage gap. By similar styles of grouting these cut-off walls, Mansuri et al. (2014) proposed hydraulic barriers at dam foundation via sufficient head loss that decreases uplift pressure and reduces the exit gradient. Even so, inclined cut-off wall is better than vertically grouted type. In this respect, the cut-off columns will effectively cover the seepage pathway modeled in Fig. 10, if placed in inclined angles from piles b to d, and from abutment e' into the downstream. Moreso, option of minimizing the initial seepages in blanketing the aquitards by cement treating the composite clay should be considered. It could be expensive (Stephens 2010) but cost-effective, especially in cases of large hydro dams. More remedial approach includes piling into the bedrock to eliminate failure uncertainties, even as $FS \geq 2.5$ would limit settlements empirically.

Conclusions

In the studied area, overlapping geologic formations of wide age gap from Lower Cretaceous Albian Asu River Shales to Coniacian Agbani Sandstones of Upper Cretaceous era has induced geotechnical imbalances that affected the stability of the studied dam. Ezeaku Group of Turonian age is adjudged weaker rock mass than the older Asu River Shale; yet, both formed stable bearing surfaces for heavy structure foundations like the dam. But presence of an intermediate layer formed by clay/silt that marked lower limit of subgrades influenced strength of overall composite shale bedrocks, particularly at an unconforming boundary between the eras. The clay/silt layer which overlies the shales directly produced aquitard underneath the dam, and raised hydrologic condition which initiated instability of the dam structure. This is because the

aquitards formed regional seepage pathway and were undercut at depression-like and subgrade-filled unconformed boundary gap. Sagging and subsequent filling of the gap is more severed towards weaker Ezeaku Group, and was attributed to devastations of the shales by weathering effect of trapped seeped water. The trapped pore water therefore mounded, thereby raising energy head locally towards and above the water table, and with slight increase in density due to concentration of salinity (dissolved solutes) by ARD, uplift pressure (P_u) was established to inflate self-weight of the dam (D_w). The compromised self-weight yielded to instability, resulting in geotechnical uncertainties, particularly in form of settlement on the portion of tail water embankment. This caused vigorous leakages of the tailwater into the dam foundation. Predictably, the leakage will further initiate critical exit gradient due to heightened hydraulic head at tail water axis, and would spread across the foundations of the dam. Thus, general shear failure is envisaged if the hydrogeological condition is not checked, especially as the end bearing is vulnerable to corrosion induced by dissolved iron. The iron mineral was advected through the leakages to form part of chemical agents that reacted with pore water to weaken the bearing surfaces via chemical weathering. Remedial measures like grouting with quality cement as an admixture in treating the clayey subgrade-filled leakage axis for consolidation purpose as well as construction of cut-off wall into the graben-like local shear zone beneath the dam using standard stress-resistant modes, particularly choosing an appropriate $FS \geq 2.5$, and presumptive measure like $P_u < D_w$ can be established as criteria for routine check of internal stability of the dam. This would be achieved by routine measurement of the uplift force (P_u) with respect to the designed weight of the dam (D_w). The cored holes used for sampling can be developed as monitoring wells around the dam foundation for groundwater (or pore water) level monitoring to check and curb the uplift force.

Therefore, in general cases of iron-banded terrain, with clay-laden subgrades, overlapped sediments, and other geological/hydrological situations like that of the studied damsite, integration of the aforementioned restorative measures would be panacea to possible geotechnical instability. Typically, these sensitive situations should be considered during preliminary investigation of sites for construction of dams, even as the suggested remedial approaches could be incorporated in maintenance activities, especially in larger than local schemes.

Supplementary Information The online version of this article (<https://doi.org/10.1007/s10064-020-01977-7>) contains supplementary material, which is available to authorized users.

Acknowledgments The author is grateful to Mr. Fashoto Ayodele of MAPREF GEOTECHNICAL LTD and Mr. G. Babadiya of Geotechnical Laboratory, Ministry of Works, Abakaliki, Nigeria, for the rock in situ tests and analyses. Mr. Ani, C.C of Department of Geology/Exploration Geophysics, Ebonyi State University, Abakaliki,

has been appreciated for conducting and analyzing the geophysical data. I am indebted to Miss Okparaugo Chisom for assisting in geological mapping. Most special thanks go to the editor-in-chief and the entire editorial crew, as well as the erudite reviewers of *Bulletin of Engineering Geology and the Environment* for lots of contribution that enhanced the quality of this manuscript.

References

- Akande SO, Hoffknecht A, Erdtmann BD (1992) Rank and petrographic composition of selected Upper Cretaceous and Tertiary Coals of Southern Nigeria. *Int J Coal Geol* 20:209–224
- Akpaodiogaga P, Ovuyovwiroye O (2010) General overview of climate change impact in Nigeria. *J Hum Ecol*, Taylor and Francis online 29(1):47–55.
<https://doi.org/10.1080/0p709274.2010.11906248>
- Altinbilek A (2002) The role of dams in development. *Int J Water Resour Dev* 18(1):9–24.
<https://doi.org/10.1080/07900620220121620>
- American Society of Civil Engineers (ASCE) (2017) Infrastructure report card: a comprehensive assessment of America's Infrastructure, p 110. Accessed on 29/11/2019, at:
<http://www.infrastructurereportcard.org/wp-content/uploads/2019/02/full-2017-Report-card-final.pdf>
- Association of State Dam Safety Officials (ASDSO) (2019) Dam failures incidents, ASDSO Conference proceedings, Orlando, USA. Viewed at:
damsafety.org/dam-failures
- Bangladesh National Building Code, BNBC (2012) Structural design part 6, chapter 3: soil and foundation, 2:152–224
- Beck MW, Claassen AH, Hundt PJ (2012) Environmental and livelivelihood impact of dam: common lessons across development gradient that challenge sustainability. *Int J River Basin Manag* 10(1):73–92.
<https://doi.org/10.1080/15715124.2012.656133>
- Bieniawski ZT (1989) Engineering rock mass classifications: a complete manual for engineers and geologists in mining, civil, and petroleum engineering. John Wiley & Sons, New York, pp 272
- Benkhelil J (1989) The origin and evolution of the Cretaceous Benue Trough (Nigeria). *J Afr Earth Sci* 8:251–282
- Berry AA, Saad R, Mohamad TE, Jinmin M, Azwin IN, Akip-Tan NM, Nordiana MM (2012) Electrical resistivity and induced polarization data correlation with conductivity for iron ore exploration. *Electron J Geotech Eng Bundle W* 17:3223–3337
- Bignold GJ (2003) Structural integrity assessment – examples and case studies. Milne I, Karihaloo B, Ritchie RO (eds) In: *Comprehensive structural integrity*, vol. 1, pp 1–24
- Boyè H, de Vivo M (2016) The environmental and social acceptability of dams. *J Field Actions Sci Rep* 9(14)
- Briaud J-L (2013) Geotechnical engineering: saturated and unsaturated soils. Wiley, New Jersey 969p
- Brown ET (1981) International Association of Rock Mechanics (ISRM) suggested methods- rock characterization testing and monitoring. Pergamon Press, Oxford
- Burke K, Dewey JF (1974) Two plates in Africa during the cretaceous? *Nature* 249:313–316
- Burke K, Whiteman AJ (1973) Uplift, rifting and the break-up of Africa. In: Tarling DH, Runcorn SK (eds) *Implications of continental drift to the Earth Sciences*. Academic, London, pp 735–755
- Burke KC, Whiteman AJ, Dessauvage TFJ (1970) Geological history of the Benue Valley and the adjacent areas. In: Dessauvage TFJ, Whiteman AJ (eds) *African Geology*. Ibadan University Press, Ibadan, pp 187–205
- Chilton J (1996) Groundwater. In: Chapman D (ed) *Water quality assessment- a guide to biota, sediments and water in environmental monitoring*, Chapter 9, 2nd edn. UNESCO/WHO/UNEP
- Chipperfield JR (2003) Iron: properties and determination. In: Caballero B (ed) *Encyclopedia of Food Science and Nutrition*, 2nd edn, pp 3367–3373
- Chu A, Stumm F, Joesten PK, Noll ML (2013) Geophysical and hydrologic analysis of an earthen dam site in southern Westchester County. U.S. Geological Survey Scientific Investigations Report 2012–5247, New York p 64. (Available at
<http://pubs.usgs.gov/sir/2012/5247/>)
- Coduto DP (1994) Technology and engineering. In: *Foundation design: principles and practices*. Prentice Hall, Englewood Cliff, pp 796
- Costa JE (1985) Flood from Dan failure. U. G Geological Survey Open-File Report 85–560, Denver, Colorado, 54p
- Don DR, Malcolm JB, Michael JK (2009) *Water supply*, 6th edn. 744p.
<https://doi.org/10.1016/B978-0-7506-6843-9.x0001-7>
- Duarte IMR, Gomes CSF, Pinho AB (2018) Chemical weathering. In: Bobrowsky PT, Marker B (eds) *Encyclopedia of engineering geology*. *Encyclopedia of Earth Sciences Series*. Springer, Cham.
<https://doi.org/10.1007/978-3-319-73568-9>
- Ethan O, Weikel PG (2008) Repeatability and reliability of fracture trace analysis, and the use of multiple analysis sources with independent validation to add confidence to fracture trace results. 17th annual Maryland Groundwater symposium. SAIC, from science to solution
- Ezeigbo HI (2003) Towards sustainable potable water supply to Nigerias in the new millennium. In: Elueze AA (ed) *Contribution to Geosciences and mining to National Development*. Nigerian mining and Geosciences Society, pp 19–23
- Fetter CW (2007) *Applied hydrogeology*, 2nd edn. CBS Publishers, New Delhi, 592p
- Fooks PG, Lee EM (2019) Engineering geology of concretes in hot dryland. *Q J Eng Geol Hydrogeol* 52(3):257–279.
<https://doi.org/10.1144/qjgeh.2018-185>
- Freeze AR, Cherry JA (1979) *Groundwater*. Prentice Hall Inc., Englewood Cliff, pp 604
- Ga'NE (2000) The impact of acid -mine drainage on groundwater quality, Davis Pyrite Mine, Massachusetts Doctoral Dissertations Available from:
<https://scholarworks.umass.edu/dissertations/AAI9988783>. Accessed 20 Dec 2019
- Gance J, Sailhac P, Malet JP (2015) Corrections of Surface fissure effect on apparent resistivity measurements. *Geophys J Int* 200(2):1118–1135
- Gholami R, Fakhari N (2017) Support vector machine – principles, parameters and applications. In: Samui P, Sekhar S, Balas VE (eds) *Handbook on neural computation*, Ch. 27, pp 515–535
- Goodman RE (1989) *Introduction to rock mechanics*, 2nd edn. Wiley, New York, 576p
- Goodman RE (1993) *Engineering geology: rocks in engineering construction*. Wiley, New York 432p
- Hoek E, Kaiser PK, Bawden WF (1995) *Support of underground excavations*. A.A Balkema Publ., Rotterdam ISBN 10:9054101865
- Hwang RN, Ishihara K, Lee WF (2016) Forensic studies for failure in construction of and underground station of the Kaohsiung MRT System. In: *Forensic Geotechnical Engineering*. Springer, New Delhi, pp 357–368
- Idowu JO, Ekweozor CM (1993) Petroleum potential of Cretaceous shales in the Upper Benue Trough, Nigeria. *J Pet Geol* 16(3):249–264
- Indian Standard IS (1987) Code of practice for design and construction of shallow foundation on rocks. IS 12070, Bureau of Indian Standard
- International Society for Rock Mechanics (ISRM) (1981) Basic geological description of rock masses. *Int J Mech Min Sci Geomech, Abstr* 18:85–110

- ISRM (2007) The complete ISRM suggested methods for rock characterization, testing and monitoring: 1974-2006. International Society for Rock Mechanics, Commission on Testing Methods. Turkish National Group, Ankara 628p
- Kawasaki S, Tanimoto C, Koizumi K, Ishikawa M (2002) An attempt to estimate mechanical properties of rocks using the Equotip hardness tester. *Jpn Soc Eng Geol* 43:244–248
- Klein JD, Sill WR (1982) Electrical properties of artificial coal bearing sandstone. *Geophysics* 47(11):1593–1605
- Kvamme B, Kuznetsova T, Kivela P-H (2012) Adsorption of water and carbon dioxide on hematite and consequences for possible hydrate formation. *Phys Chem Chem Phys* 14(13):4410–4424. <https://doi.org/10.1039/c2cp23810a>
- Lelièvre PG, Farquharson CG (2013) Gradient and smoothness regularization operators for geophysical inversion on unstructured meshes. *Geophys J Int* 178:623–637
- Loke MH (1999) A practical guide to 2D and 3D surveys. *Electrical Imaging Surveys for Environmental and Engineering Studies*, p 8–10
- Loke MH (2001) Electrical imaging surveys for environmental and engineering studies. A practical guide to 2-D and 3-D surveys: RES2DINV manual. Geotomo Software, Malaysia, p 127. www.geoelectrical.com. Accessed 01 Apr 2018
- Look BL (2007) Handbook of geotechnical investigation and design tables. *Proceedings and Monographs in Engineering, Water and Earth Science*, Balkema. Chapter 6: rock Strength parameters from classification and testing Taylor and Francis online, pp 65–76
- Lyons DJ, Van deCamp PC (1980) Subsurface geological and geophysical study of Cerro Prieto geothermal field, Baja California, Mexico. Earth Science Division, University of California, Oakland 91p
- Mansuri B, Salmasi F, Oghati B (2014) Effect of location and angle of cut-off wall on uplift pressure in diversion dam. *Geotech Geol Eng* 32:1165–1173. <https://doi.org/10.1007/s10706-014-9774-3>
- Marinos P, Hoek E (2000) GSI: a geologically friendly tool for rock mass strength estimation. In: *Proceedings of GeoEng 2000 at the International Conference on Geotechnical and Geological Engineering*, Australia. Technomic Publishers, Lancaster, pp 1422–1446
- Marinos P, Hoek E (2001) Estimating the geological properties of heterogeneous rock masses such as flysch. *Bull Eng Geol Environ* 60: 85–92
- Martin CJ, Morley AL, Griffiths JS (2017) Introduction to engineering geology and geomorphology of glaciated and periglacial terrains Chapter 1. *Geol Soc Lond Eng Geol Spec Publ* 28:1–30. <https://doi.org/10.1144/EGSP28.1>
- New York State Department of Environmental Conservation (NYSDEC) (2009) Dam hazard classification. Bureau of Flood Protection and Dam Safety, 6CRR-NY673.5
- Nwajide CS (2005) Anambra Basin of Nigeria: synoptic basin analysis as a basis for evaluating its hydrocarbon Prospectivity. In: Okogbue CO (ed) *Hydrocarbon potentials of Anambra Basin*, Proceedings of the Petroleum Technology Development Fund (PTDF) Chair in geology. University of Nigeria, Nsukka, pp 1–46
- Nwajide CS (2013) *Geology of Nigeria's sedimentary basins*. CSS Press, Lagos, 565p
- Obaje NG (2009) *Geology and mineral resources of Nigeria*. Springer-verlag, Berlin Heidelberg 221p
- Ofoegbu CO, Odigi MI, Ebeniro JO (1990) The tectonic evolution of the Benue Trough. In: Ofoegbu CO (ed) *The Benue Trough. Structure and Evolution*. Vieweg and Sohn, Braunschweig, pp 203–216
- Okogbue CO, Ukpai SN (2013) Evaluation of trace element contents in groundwater in Abakaliki Metropolis and around the abandoned mine sites in the southern part, Southeastern, Nigeria. *Environ Earth Sci*, springer 70:3351–3362
- Okoro A (2016) Sedimentary and petrofacies analyses of the Amasiri Sandstone, southern Benue Trough, Nigeria: implications for depositional environment and tectonic provenance. *J Afr Earth Sci* 123: 258–271
- Onyedim GC (2007) Mapping faults in part of Benue Trough, Nigeria by cross correlation analysis of gravity data. *J Appl Sci* 7(2):226–231. <https://doi.org/10.3923/jas.2007226.231>
- Osouli A, Bajestani BM, Shafii I, Singh KS (2014) Conversion of point load test results to conventional strength tests for shale, claystone and limestone rocks. *American Rock Mechanoc Association (ARMA-14- 7424)*. 48th US Rock Mechanics / Geomechanics Symposium held in Minneapolis, MN, USA
- Oude Essink GHP (2001) Hydrological transport processes/groundwater modelling II. In: *Density dependent groundwater flow -salt water intrusion and heat transport, KHTP/GWM II: L3041/L4019*, 137p
- Pan Y, Fu Y (2020) Effect of random geometric imperfections on the water-tightness of diaphragm wall. *J Hydrol* 580:124252. <https://doi.org/10.1016/j.hydrol.2019.124252>
- Pan Y, Liu Y, Hu J, Sun M, Wang W (2017) Probabilistic investigations on the watertightness of jet-grouted ground considering geometric imperfections in diameter and position. *Can Geotech J* 54(10):1447–1459
- Panthulu TV, Krishnaiah C, Shirke JM (2001) Detection of seepage paths in earth dams using self-potential and electrical resistivity methods. *Eng Geol* 59(3):281–295. [https://doi.org/10.1016/S0013-7952\(00\)0082-X](https://doi.org/10.1016/S0013-7952(00)0082-X)
- Peters SW, Ekweozor CM (1982) Petroleum geology of the Benue Trough and Southeastern Chad Basin, Nigeria. *Am Assoc Pet Geol Bull* 66:1141–1149
- Prucha JJ (1992) Zone of weakness concept: a review and evaluation. In: Bartholomew MJ, Hyndman DW, Mogk DW, Mason R (eds) *Basement Tectonics 8. Proceedings of the International Conferences on Basement Tectonics*, vol 2. Springer, Dordrecht. https://doi.org/10.1007/978-94-011-1614-5_7
- Rajapakse R (2016) *Geotechnical Engineering Calculations of Tnomb*, 2nd edn. Elsevier, Amsterdam, 508p. <https://doi.org/10.1016/C2015-0-01445-9>
- Rehman F, Abouelnaga H, Harbi H, Cheema T, Ali HA (2016) Using a combined electrical resistivity imaging and induced polarization techniques with the chemical analysis in determining of groundwater pollution at Al Misk Lake, Eastern Jeddah, Saudi Arabia. *Arab J Geosci* 9. <https://doi.org/10.1007/s12517-016-2423-9>
- Roberge PR (2006) *Corrosion basics: an introduction*, 2nd edn. NACE Press Book, Houston 364p
- Robert CM (2009) *Global sedimentology of the ocean: an interplay between geodynamic and paleoenvironment*, vol 4. Elsevier, Amsterdam 241p
- Roclab A (2006) Roclab Computer Program. From Rocscience website: www.rocscience.com. Accessed 22 Oct 2019
- Rusnak J, Mark C (1999) Using the point load test to determine the uniaxial compressive strength of coal measure rock. In *Proceedings of 19th international conference on ground control in mining*, pp 362–371
- Scholz M (2006) *Wetland system to control urban run off*. University of Edinburgh, Edinburgh., 360p. <https://doi.org/10.1016/B978-0-444-52734-9.X5000-2>
- Shah Shahrbanouzadeh M, Barani GA, Shojae S (2015) Analysis of flow through dam foundation by FEM and ANN models: case of Shahid Abbaspour Dam. *Geomech Eng* 9(4):465–481. <https://doi.org/10.12989/gae.2015.9.4.465465>
- Sheets RA (2002) Use of electrical resistivity to detect underground mine voids in Ohio, U.S. Geological Survey, Water-Resources Investigations Report 02–4041, p 10
- Singh B, Goel RK (2011) Engineering rock mass classification-tunneling, foundation and landslides. In: *Chapter 20: Allowable bearing*

- pressure for shallow foundation. Elsevier Inc., Amsterdam, pp 267–280.
<https://doi.org/10.1016/B978-0-12-385878-8.00020-3>
- Sissakian VK, Adamo N, Al-Ansari N (2020) The role of geological investigations for dam siting: Mosul Dam a case study. *Geotech Geol Eng* 38:2085–2096.
<https://doi.org/10.1007/s10706-019-01150-2>
- Sitharam TG (2019) Advanced foundation engineering. In: Chapter 2: shallow foundations. Taylor and Francis, Abingdon 432p
- Sivakugan N, Das BM, Lovisa J, Patra CR (2014) Determination of and of rocks from indirect tensile strength and uniaxial compression tests. *Int J Geotech Eng* 8(1):59–65.
<https://doi.org/10.1179/1938636213Z.00000000053>
- Sivakumar B (2011) Water crisis: from conflict to cooperation—an overview. *Hydrol Sci J* 56(4):531–552.
<https://doi.org/10.1080/02626667.2011.580747>
- Stephens T (2010) Manual on small earth dams: a guide to siting, design and construction. Food and Agricultural Organization (FAO) Irrigation and Drainage paper 64; Ch.6: Detailed Design, pp 43–60
- Tan Y, Lu Y (2017) Forensic diagnosis of a leaking accident during excavation. *J Perform Constr Facil* 31(5):4017061
- Tiren SA (2012) Identification of brittle deformation zones and weakness zones, Stral Sakerhets Myndigheten, Swedish Radiation Safety Authority, Report number: 2012:71, p 223.
- Todd DK (1980) Groundwater hydrology. John Wisely and Sons Inc., New York 535p
- U.S Department of Interior, Bureau on Reclamation (USBR) (2014) Embankment dams: seepages, phase 4, DS-13 (8) – 4.1
- Ukpai SN (2018) Integration of geophysical with hydrogeological methods. European University Editions: International Book Market Service Ltd, Omniscryptum Publ. Beau Bassin Mauritius, 238p. ISBN: 978–3–330-87537-1
- Ukpai SN, Okogbue CO (2017) Geophysical, geochemical and hydrological analyses of water-resource vulnerability to salinization: case of the Uburu-Okposi salt lakes and environs, Southeast Nigeria. *Hydrogeol J*.
<https://doi.org/10.1007/s10040-017-1604-2>
- Ukpai SN, Nnabo PN, Eze HN (2016) Groundwater facie analysis of Upper Cross River Basin, Southeast Nigeria. *Environ Earth Sci* 75(20):1345–1355.
<https://doi.org/10.1007/s12665-016-6139-7>
- Ukpai SN, Eze HN, Igwe JO (2017) Aquifer prospect and vulnerability of Upper Maastrichtian sandstones: case of Ajali and Nsukka formations in the Northern Enugu Province, southeastern Nigeria. *J Afr Earth Sci* 135:96–107
- Ukpai SN, Okogbue CO, Oha IA (2019) Investigation of hydrologic influence of geologic lineaments in areas of the Lower Benue Trough, Southeastern Nigeria. *J Earth Syst Sci* 129:12.
<https://doi.org/10.1007/s12040-019-1283-6>
- Umaji OP (1984) Ammonite palaeontology of the Ezeaku Formation, Southeastern Nigeria. *J Min Geol* 22(1 & 2):55–59
- Umaji OP (2002) Mid-Tertiary (Late Eocene-Early Miocene) lignites from MPU Formation, Abakaliki basin, southeastern Nigeria. *J Min Geol* (38):111–118.
<https://doi.org/10.4314/jmg.v.382.18781>
- United States Geological Survey (USGS) (2016) Landsat—Earth observation satellites (ver. 1.1.): USGS Fact Sheet 2015–3081, 4 p.,
<https://doi.org/10.3133/fs20153081>. ISSN: 2327-6932 (online)
- Vardanega PJ, Bolton MD (2013) Stiffness of clays and silts: normalizing shear modulus and shear strain. *J Geotech Geoenviron Eng* 139(9): 1575–1589.
[https://doi.org/10.1061/\(ASCE\)GT.1943-5606.0000887](https://doi.org/10.1061/(ASCE)GT.1943-5606.0000887)
- Wahl TL (1998) Prediction of embankment dam breach parameters. A literature review and assessment. Dam Safety Service [DSO-98-004], Water Research Laboratory, U.S Department of interior. 60p
- Waltham AC (1994) Foundations of engineering geology. Blackie Academic and Professionals, London 88p
- Wang H, Lin H, Cao P (2016) Correlation of UCS rating with Schmidt hammer surface hardness for rock mass rating. *Rock Mech Rock Eng* 50(1).
<https://doi.org/10.1007/s00603-016-1044-7>
- Wright JB (1989) Volcanic rocks in Nigeria. In: Kogbe CA (ed) *Geology of Nigeria*, 2nd revised edn. Rock View (Nigeria) Ltd., Jos, Nigeria, pp 125–173
- Yao K, Pan Y, Jia L, Yi JT, Hu J, Wu C (2019) Strength evaluation of marine clay stabilized by cementitious binder. *Mar Georesour Geotechnol*.
<https://doi.org/10.1080/1064119X2019.1615583>
- Yao K, Chen Q, Xiao H, Liu Y, Lee FH (2020) Small-strain shear modulus of cement-treated marine clay. *J Mater Civ Eng* 6(32): 04020114.
[https://doi.org/10.1061/\(ASCE\)MT.1943-5533.0003153](https://doi.org/10.1061/(ASCE)MT.1943-5533.0003153)
- Zainab M, Kamaruzaman M, Haryati A (2007) Empirical strength and stiffness models for composite rock of weathered sandstone and shale components. *Electron J Geotech Eng* 12:0703C
- Zhang L (2004) Drilled shaft in rocks: analysis and design. Taylor and Francis Group, Abingdon 377p
- Zhou J, Revil A, Karaoulis M, Hale D, Doetsch J, Cuttler S (2014) Image-guided inversion of electrical resistivity data. *Geophys J Int* 197(1): 292–309.
<https://doi.org/10.1093/gji/ggu001>